Hydrol. Earth Syst. Sci. Discuss., 10, 13897–13953, 2013
www.hydrol-earth-syst-sci-discuss.net/10/13897/2013/
doi:10.5194/hessd-10-13897-2013

Hydrology and Earth System Sciences
Open Access
Discussions

Irrigated plantations and their effect on energy fluxes in a semi-arid region of Israel – a validated 3-D model simulation

O. Branch[1], **K. Warrach-Sagi**[1], **V. Wulfmeyer**[1], **and S. Cohen**[2]

[1]Institute of Physics and Meteorology, University of Hohenheim, Stuttgart, Germany
[2]Institute of Soil, Water and Environmental Sciences, Agricultural Research Organization, Volcani Center, Bet Dagan, Israel

Received: 27 September 2013 – Accepted: 30 October 2013 – Published: 15 November 2013

Correspondence to: O. Branch (oliver_branch@uni-hohenheim.de)

Published by Copernicus Publications on behalf of the European Geosciences Union.

Abstract

A large irrigated biomass plantation was simulated in an arid region of Israel within the WRF-NOAH coupled atmospheric/land surface model in order to assess land surface atmosphere feedbacks. Simulations were carried out for the 2012 summer season (JJA). The irrigated plantations were simulated by prescribing tailored land surface and soil/plant parameters, and by implementing a newly devised, controllable subsurface irrigation scheme within NOAH. Two model cases studies were considered and compared – *Impact* and *Control*. Impact simulates a hypothetical 10 km × 10 km irrigated plantation. Control represents a baseline and uses the existing land surface data, where the predominant land surface type in the area is bare desert soil. Central to the study is model validation against observations collected for the study over the same period. Surface meteorological and soil observations were made at a desert site and from a 400 ha *Simmondsia chinensis* (Jojoba) plantation. Control was validated with data from the desert, and Impact from the Jojoba. Finally, estimations were made of the energy balance, applying two Penman–Monteith based methods along with observed meteorological data. These estimations were compared with simulated energy fluxes.

Control simulates the daytime desert surface 2 m air temperatures (T2) with less than 0.2 °C deviation and the vapour pressure deficit (VPD) to within 0.25 hPa. Desert wind speed (U) is simulated to within 0.5 m s^{-1} and the net surface radiation (R_n) to 25 W m^{-2}. Soil heat flux (G) is not so accurately simulated by Control (up to 30 W m^{-2} deviation) and 5 cm soil temperatures (ST5) are simulated to within 1.5 °C. Impact simulates daytime T2 over irrigated vegetation to within 1–1.5 °C, the VPD to 0.5 hPa, R_n to 50 W m^{-2} and ST5 to within 2 °C. Simulated Impact G deviates up to 40 W m^{-2}, highlighting a need for re-parameterisation or better soil classification, but the overall contribution to the energy balance is small (5–6 %). During the night, significant T2 and ST5 cold biases of 2–4 °C are present. Diurnal latent heat values from WRF Impact correspond closely with Penman–Monteith estimation curves, and latent heat

HESSD
10, 13897–13953, 2013

magnitudes of 160 W m^{-2} over the plantation are usual. Simulated plantation sensible heat fluxes are high (450 W m^{-2}) – around 100–110 W m^{-2} higher than over the surrounding desert. The high relative HFX over the vegetation, driven by high R_n and high surface resistances, indicate that low Bowen ratios should not necessarily be assumed when irrigated plantations are implemented in, and optimized for arid regions. Furthermore, the high plantation T2 magnitudes highlight the importance of considering diurnal dynamics, which drive the evolution of boundary layers, rather than only on daily mean statistics which often indicate an irrigation cooling effect.

1 Introduction

The large scale implementation of biomass plantations in arid regions is the subject of recent research due to perceived potential for carbon sequestration, energy production, agricultural development and environmental services (Becker et al., 2013; Beringer et al., 2011). Such plantations are becoming feasible through modern desalination (Khawaji et al., 2008; Fritzmann et al., 2007), wastewater (Hamilton et al., 2007; Oron et al., 1999), and irrigation techniques, e.g. see Spreer et al., (2007). Valuable and hardy shrubs such as *Jatropha curcas* or *Simmondsia chinensis* (Jojoba) can withstand heat and drought, and be irrigated with waste- or brackish water (Rajaona, 2012; Abou Kheira and Atta, 2009; Benzioni, 2010). These traits makes them more viable than many food crops and may reduce threats to food security if exclusive use of marginal land is adhered to Becker et al. (2013).

Critical research is still missing however, on potential climatic impacts caused by significant land surface modifications in arid regions. Vital insights can be obtained using dynamically downscaled simulations with coupled atmospheric/land surface models. Such models need careful calibration for regional arid conditions though, and validation to assess confidence in simulation results.

Large-scale agroforestry (AF) could modify the local and regional climate. Alpert and Mandel (1986), observed a reduction in amplitude and variance of wind speeds (U)

HESSD
10, 13897–13953, 2013

and 2 m temperatures (T2) in Israel over 3 decades. They correlated changes with increases in irrigation since the 1960s, and attribute them to lower sensible heat fluxes (HFX) and changes in albedo and roughness. Ridder and Gallée (1998) concurred with these trends. Increases in rainfall, especially around October were also found (Ben-Gai et al., 1993, 1994, 1998; Otterman et al., 1990) in Perlin and Alpert (2001). This is likely due to the combination of autumn climatic conditions and the land surface perturbations. From Ridder and Gallée (1998), Alpert and Mandel conclude that altered weather patterns are caused by lower HFX from irrigated cops, whereas Otterman cites increased HFX from non-irrigated shrubs. For the latter land use type, higher Bowen ratios would result from less water availability. Otterman also found that increased Saharan fringe vegetation increased daytime convection and atmospheric boundary layer (ABL) growth.

Given the likely dependence of flux partitioning on soil moisture, this presents some interesting questions to investigate: What effect will large irrigated plantations have on the mesoscale climate? What scale of plantations will induce significant effects? What partitioning of fluxes can be expected from a large arid irrigated plantation? How would these fluxes contrast with the surrounding desert surface?

The introduction of large vegetation patches into deserts is likely to induce significant horizontal flux gradients, increase surface roughness, moisten the ABL, modify turbulent flows, and induce pressure perturbations. These phenomena would influence ABL evolution and may cause convergences (Wulfmeyer et al., 2013) and mesoscale circulations (Hong, 1995; Mahfouf et al., 1987). Impacts could be dependent on the scale of the patches. Dalu et al. (1996) suggests flux gradients of the order of 1 to 10 km are sufficient to induce significant changes. Letzel and Raasch (2003) estimate scales of around 5 km from LES simulations. Contiguous plantations on scales of this order could be feasible now for the reasons previously discussed.

Regarding fluxes, an expectation is that a freely transpiring canopy would result in low Bowen ratios in contrast to bare desert surfaces, where latent heat (LH) is likely to be almost zero. However, it is not clear how plantation HFX magnitudes would compare

HESSD
10, 13897–13953, 2013

with typically high desert HFX. Firstly, there is generally a greater surface net radiation (R_n) at canopy surfaces due to lower albedos. Secondly, leaves can be very efficient heat radiators, and have lower heat storage potential than most substrates (Giles, 2006). Finally, desert crops such as Jojoba or Jatropha may not transpire freely due to their high water use efficiency and resistance to water stress (Silva et al., 2010; Abou Kheira and Atta, 2009; Benzioni and Dunstone, 1988) and also because efficient irrigation techniques such as partial root zone drying are used (Spreer et al., 2007). The final point is significant, because in arid regions a fine balance exists between maintaining yield and plant health, and the need to conserve water. Plantation evapotranspiration (ET) could therefore be limited, resulting in higher Bowen ratios than a freely transpiring canopy implies. An example of large HFX magnitudes from drier vegetation is the Yatir pine forest in Israel, where Rotenberg and Yakir (2010) observed summer HFX magnitudes that were 1.3 times higher than over the Sahara and 1.6 and 2.4 times higher than tropical and temperate forests, respectively.

Relative HFX over plantation and desert will depend largely on the albedos and energy balance over the plantation. In turn, albedo generally depends on crop type, phenological stage, canopy cover, senescent material and so forth. ET depends not only on water availability, soil characteristics and boundary layer conditions, but also on roughness and plantation/canopy/leaf homogeneity, geometry and scale. Specific plant characteristics and survival strategies also play a major role, such as modified photosynthesis pathways or stomatal closure. This is especially true with many desert species.

In order to estimate impacts on atmospheric interactions, detailed simulations are carried out within coupled atmospheric and land surface models (LSM). This can be achieved by artificially modifying the land surface data used by the LSM to calculate surface exchanges. If the model is correctly parameterized, we can assess impacts on (a) diurnal fluxes, (b) feedbacks to and from the ABL, and (c) larger scale impacts such as convection initiation. Furthermore, certain variables can be tested such as plantation size and location.

HESSD
10, 13897–13953, 2013

The use of coupled 3-D models is desirable because, unlike uncoupled models they can simulate bi-directional feedbacks, from the soils to the entrainment zone. These process are central to ABL evolution (e.g. see Van Heerwaarden et al., 2009), evaporation and therefore flux gradients over heterogeneous landscapes. The use of fine resolutions of e.g. < 4 km, allow for detailed resolution of landscape features and can reduce systematic errors and biases in soil-cloud-precipitation feedbacks commonly seen in coarser models where convection is normally parameterized (Rotach et al., 2009, 2010; Wulfmeyer et al., 2011, 2008; Bauer et al., 2011; Weusthoff et al., 2010; Schwitalla et al., 2008).

Our ultimate goal is to use the WRF-NOAH model to conduct impact studies on meso α scales. This study focuses on the parameterization and validation of the WRF (Skamarock et al., 2005) with its LSM NOAH (Chen and Dudhia, 2001) model for the region/vegetation/irrigation/soils, and also on the comparison of energy fluxes over the desert and plantation. Two model scenarios are set-up – WRF Control and WRF Impact. WRF Control represents a baseline, using unmodified MODIS land surface type initialisation data and the second is a simulation of a 10 km × 10 km irrigated plantation (WRF Impact). WRF Control output is compared to observations from a desert surface and WRF Impact is compared with observations from the Jojoba plantation. These observations were collected especially for the experiment. Specific objectives are:

- conduct an experimental study, to form the basis for a model configuration for later impact studies on large scale arid plantations,
- build and set up a WRF-NOAH model simulation for irrigated plantations in a semi-arid region,
- to validate the model for follow-up impact studies.

HESSD
10, 13897–13953, 2013

2 The study area and its climate

The impact of plantations is studied in the semi-arid region of Israel. In this area, long hot summers, clear skies and high radiation are the most common conditions. Synoptically, a pressure trough to the north generally runs from Turkey down to the Persian Gulf drawing north-north-western winds steadily in from the Mediterranean for most of the year. Until around October, the summer climate is dominated by Hadley subsidence and strong inversions, which inhibit convection. Afterwards, these inversions tend to weaken, after which time the Mediterranean and its winter cyclones starts to have more influence. Precipitation is usually convective when it occurs, either embedded in the passage of fronts or induced by local circulations (Perlin and Alpert, 2001).

This study focuses on the area of the northern edge of Israel's Negev Desert close to the city of Beer'sheva (see Fig. 1 – inset) around 50 km from the coast (31.242309° N, 34.721620° E). This lies roughly on the border of two climatic zones – a semi-arid one with crops and grasslands to the north, and an arid one to the south. In this desert area various plantations exist. Among them are a Jatropha and a Jojoba plantation, which are the subject of this investigation and as a control case, a dry desert area was chosen. All cases are located approximately 2 km to the west of Beer'sheva.

The "Desert" case study is situated on a bare, desert soil with no vegetation, marked (1) in Fig. 1. Some small plantations exist around 800 m upwind but it is assumed that moisture advection to the sensors would not be significant, and that non-advected quantities such as surface radiation and soil temperature would be representative of a desert surface. The "Jatropha" case study (2) is a 2 ha irrigated *Jatropha curcas* plantation and the "Jojoba" case study (2) is a 400 ha plantation of irrigated Jojoba with a canopy height of around 3–3.5 m. Both plantations are irrigated with secondary treated waste water from Beer'sheva, with low water salinity, i.e. the plantation's managers report that mean electrical conductivity (EC) of the irrigation water is $\sim 1\,\mathrm{dS\,m^{-1}}$ (see Appendix B for more information about salinity). The experimental Jatropha plantation is irrigated only from March to December and is heavily pruned during the winter.

HESSD
10, 13897–13953, 2013

Because of this, the canopy cover is still only around 50–60 % at the beginning of June. This increased over the summer to nearly 100 % during July. This is likely to bias the Jatropha observations somewhat (compared to a fully mature Jatropha canopy) due to gradual changes in wind speed, albedo, evaporation and so on. Due to the small size of the Jatropha plantation, and the changing canopy conditions it was decided that only the Jojoba observations would be used for validation. The Jatropha observations are however, examined and compared with the Jojoba (see Sect. 3.2) and yielded interesting information on differences in solar and thermal radiation components between the crops.

The Jojoba plantation is fully mature and watered all year round. The shrubs are widely spaced for mechanized harvesting (4 × 2.5 m) producing a canopy coverage of around 70 % for the mature sections. These factors consequently, are likely to produce differences in albedo, wind flow, turbulence, evaporation, skin and air temperatures and other quantities, when compared with a 100 % canopy closure. The soils within the plantation are mainly composed of silty to sandy loam, loess soils by local soil survey.

While the Jatropha plantation is being tested with various sub-surface treatments, the Jojoba plantation is fed by a sophisticated, sub-surface deficit irrigation system configured to maximize water use efficiency and yield. Water requirements are estimated by agronomists using meteorology data and standard methods. The irrigation flow rates, duration and dripper spacing are optimized to minimize losses to percolation, runoff and direct evaporation. Given that (a) there is little precipitation, (b) the irrigation is sub-surface and (c) the dosage is carefully calibrated, these losses are assumed to be negligible. Therefore, based on these assumptions, only the potential and transpired evaporation terms would play a role within the NOAH evaporation equation (Appendix A). The plants are watered directly at the root ball (35 cm deep) in alternate crop rows. Soil moisture (Θ) is monitored by a sensor network, and constrained to between 0.16 and 0.30 so that the plant is neither water-stressed nor over-watered. This means that the frequency of watering can be irregular depending on environmental conditions such as radiation magnitudes, phenological stage and so on. The stem spacing of the Jojoba

HESSD
10, 13897–13953, 2013

plantation also means that soil moisture is highly heterogeneous spatially. All technical information on irrigation was made available by the plantation agronomists.

3 Measurements

3.1 Site description

Meteorological data was collected at the three case study sites especially for the experiment and are named: *Desert*, *Jatropha* and *Jojoba*. Within the plantations, care was taken to site Jatropha and Jojoba well away from the plantation edges and with a substantial fetch with respect to the mean wind flow. All variables were measured with a scan rate of 5 s and averaged over 10 min intervals (see Table 1).

3.2 Analysis of observations

The summer time series from Desert, Jatropha and Jojoba (Fig. 2) reveal a general seasonal T2 pattern, peaking in July with daily means being 2–3 °C warmer than in June. Desert is warmer at night but cooler during the daytime than the plantations, with Jojoba T2 lower in general than Jatropha. Relative humidities remain fairly constant indicating more humidity during July where higher July T2 signifies higher saturation values. The Jojoba and Jatropha RH curves match very closely but Desert exhibits lower maximum RH during the night, reflecting the higher T2 minimum.

The surface air pressures (P) in Fig. 3 tend to vary inversely with the seasonal temperatures, but with large variations over periods of a few days, in accordance with changing large scale pressure systems. R_n peaks at the end of June and then decreases steadily over the season. Jojoba has a higher R_n than Jatropha especially over July, reflecting the lower albedo of Jojoba, and Desert has between 80 to 100 $W m^{-2}$ less R_n than either of the plantations. Mean U is quite constant over Desert and Jojoba, but over Jatropha they decrease somewhat over the season (0.5 $m s^{-1}$) probably

HESSD
10, 13897–13953, 2013

reflecting the Jatropha's canopy development and corresponding increase in drag. Winds speeds are in general a little higher over Jojoba than over Jatropha. There is a high variability in mean U direction and the 7 day mean indicates a slight shift of around 10° to the west through the season, for all stations. Surface wind speeds over Desert reach 5 or 6 $m\,s^{-1}$ and are in general higher than over the plantations (3–4 $m\,s^{-1}$) and also very slightly more northerly indicating the effect of drag and a tendency towards gradient flows over the canopy.

Considering mean diurnal statistics (Fig. 4), T2 values over the plantations exhibit larger amplitudes than over the desert being warmer in the daytime and cooler at night. Jatropha is warmer than the Jojoba during the day (+2 °C) and also at night (+1 or 2 °C). Day and night time RH values are fairly similar and reflect the differences in temperature over the day. Wind speeds over Desert are higher with a pronounced daytime peak late in the afternoon, 2.5 $m\,s^{-1}$ higher than the plantations. Daytime peak R_n values are around 350 $W\,m^{-2}$ higher over both plantations than over Desert, but with similar losses at night time. Daytime Jojoba albedo values are noticeably lower than the Jatropha and this is reflected in the greater Jojoba R_n values (clearly seen in Fig. 4).

4 Model simulations

This analysis is carried out via high resolution model simulations with the WRF-NOAH model. Prior to subsequent impact studies, this study focuses on the configuration and validation of the model for an arid region. Additionally, as a first examination of vegetation impacts, the energy fluxes estimated by NOAH are investigated, since these express the interaction of the atmosphere and the land surface. The model domain spans 888 km × 888 km and is centred over the state of Israel (see Fig. 5).

To judge the model performance and configuration, two cases are assessed. The first is the baseline (WRF Control). The second is a simulation of a 10 km × 10 km irrigated plantation (WRF Impact). WRF Control are compared to the Desert observations and

HESSD
10, 13897–13953, 2013

WRF Impact are compared with observations from Jojoba and Jatropha. Since our ultimate goal is to use the WRF-NOAH model to investigate the impact of horizontal flux gradients on ABL development and convection, the model should be able to reproduce these fluxes over both surfaces.

4.1 Modelling configuration

The WRF ARW (3.4.1) non-hydrostatic atmospheric model, coupled with the NOAH land surface model (LSM) was configured with a 444 × 444 cell grid with 92 vertical levels and a 2 km grid horizontal increment. A single downscaled model domain was chosen with care to capture most large scale features, such as the influx of sea air from the north-east, but to avoid orography and other strong features at the domain boundaries (see Fig. 2). The model was forced at the boundaries by ECMWF (European Centre for Medium Range Weather Forecasting) 6 hourly analysis data at 0.125° grid increment and with 6 hourly updated sea surface temperatures (SSTs). Model physics schemes were chosen based on sensitivity tests and experience with scheme stability. Additionally some schemes are designed to be paired e.g. the SW and LW RRTMG radiation schemes. The model physics schemes used are shown in Table 2.

The land surface model was initialized using the IGBP MODIS 20-category land use and soil texture with the FAO STATSGO 19 category soil dataset. The initial soil moisture state and lower soil boundary temperatures come from the forcing data. The model duration was 92 days over JJA, 2012 and instantaneous values were generated every hour. Full observation datasets from *Desert*, *Jatropha* and *Jojoba* were available for this period.

In the absence of accurate gridded initial soil moisture (Θ) conditions, a spin-up period is needed to allow soil moisture within NOAH to approach equilibrium within the hydrological cycle. The optimal spin-up period is uncertain and may depend on the application, region, accuracy of initial conditions and other factors. Du et al. (2006) simulated soil moisture in East Asia, and stated that the time interval between precipitation perturbation and reaching equilibrium is proportional to soil depth. Du states however

HESSD
10, 13897–13953, 2013

that surface soils (0–10 cm) may require a few months to reach equilibrium. However, it is likely that bare desert surface soils, with sparse precipitation will dry very quickly and there will be little atmospheric coupling with deeper layers due to the lack of roots. In the plantations, the deeper soil layers will in any case be artificially moistened. With these mitigating factors in mind, a one month (May) spin-up period was thought to be sufficient and was used here.

4.2 Irrigated plantations in NOAH

For simulation of the irrigated plantation, attention was given to the following factors: plantation location, size and shape; sub-surface irrigation scheme/soil moisture and vegetation and soil parameters. A hypothetical plantation was introduced by modifying the land surface properties in the static land surface data used by the model (see Fig. 6). A plantation size of 5 × 5 cell grid cells was used, representing dimensions of 10 × 10 km. This is in fact larger than the actual Jojoba plantation, which is closer to the size of one 2 km × 2 km grid cell. However, attempting to resolve a landscape feature with one grid cell is likely to be problematic. Independent from the model simulations, the assumption could be made that surface conditions over the 2 km × 2 km Jojoba plantation would acquire similar characteristics to those over a larger plantation of e.g. 10 km × 10 km across. This is uncertain though because, although advection effects are likely to be greatly reduced after a few hundred metres horizontally, differences in the scale of pressure perturbations and the mean wind field may well differ with the scale of the plantation. Another factor is that the wide spacing between the Jojoba plants could lead to local heterogeneities and unusual turbulent characteristics above the canopy which may differ significantly with assumptions inherent in the model. Such effects are difficult to identify with point measurements. These uncertainties should be taken into account when attempting to interpret results, where there may be deviations between modelled and measured values.

Grid cells for the plantation were first re-classified from *Desert/Scrub* to an *Evergreen Broadleaf* classification as a starting point for the configuration. Then, parameters such

HESSD
10, 13897–13953, 2013

as canopy height, minimum stomatal resistance (R_{Cmin}) and roughness were modified further based on literature on Jatropha and Jojoba, sensitivity tests and site surveys (see Table 3).

Realistic simulation of the sophisticated irrigation system of the Jojoba plantation using a soil moisture based system in NOAH is problematic, because the sub-grid heterogeneity of Θ cannot be reproduced at 2 km resolution. Nevertheless, if reasonable estimates of optimal Θ for irrigation can be made, and well-chosen plant soil and parameters are used, then we may expect a reasonable reproduction of the soil/plant water hydrology. We then make estimates of ET based on Penman–Monteith methods and observations, and compare them with the model results. These comparisons should indicate whether the irrigation scheme and parameterization produces ET of a realistic magnitude.

In order to calculate irrigation inputs, attention was paid to both the soil and plant properties. A method from Choudhury and DiGirolamo (1998) was used, who collated critical values of fractional root zone available water for various species from various publications. This value F_{AW} is the ratio of available water to maximum available water (Eq. 1):

$$F_{AW} = \frac{\Theta - \Theta_{WP}}{\Theta_{FC} - \Theta_{WP}} \quad (1)$$

where F_{AW} is the critical value, Θ_{WP} is the soil wilting point and Θ_{FC} is the field capacity. If the soil conditions, such as Θ and soil texture, are such that this ratio falls below the critical value then the plant is expected to experience stress. F_{AW} values for various species are quoted by Choudhury, but not for Jatropha or Jojoba. The variability in quoted F_{AW} values for plants of a similar biomass were not that varied – mostly between 0.3 and 0.4, with the only extremes being 0.25 for cotton and wheat and 0.50 for grasses. Sorghum, which like Jojoba and Jatropha requires a warm climate and is drought resistant, is accorded F_{AW} values of 0.37 and 0.35 by two separate studies, as reported by Choudhury. This represents the closest match in terms of climatic envelope as it can survive in semi-arid climates. Using the soil texture data a Θ value

HESSD
10, 13897–13953, 2013

of around 0.39 was calculated for F_{AW} and rounded up to 0.4. This yields a value of $0.18\,m^3\,m^3$ which was used for the irrigation target moisture level. The results should therefore be interpreted under the assumption that $0.18\,m^3\,m^3$ is the minimum permissible water input for the plants. This also relies on the assumption that the deficit irrigation techniques minimize the water quantities need for the plants to thrive.

For soil moisture transport NOAH uses a layer discretized version of the Richards equation (Eq. 2) with four soil layers of thicknesses: 10, 30, 60 and 100 cm (from the surface layer downwards). There is a free drainage scheme at the lower boundary.

$$
\begin{aligned}
d_{z_1}\frac{\partial\Theta_1}{\partial t} &= -D\left(\frac{\partial\Theta}{\partial z}\right)_{z_1} - K_{z_1} + P_D - R - E_{dir} - E_{t_1}\\
d_{z_2}\frac{\partial\Theta_2}{\partial t} &= D\left(\frac{\partial\Theta}{\partial z}\right)_{z_1} - D\left(\frac{\partial\Theta}{\partial z}\right)_{z_2} + K_{z_1} - K_{z_2} - E_{t_2} + I_E\\
d_{z_3}\frac{\partial\Theta_3}{\partial t} &= D\left(\frac{\partial\Theta}{\partial z}\right)_{z_2} - D\left(\frac{\partial\Theta}{\partial z}\right)_{z_3} + K_{z_2} - K_{z_3} - E_{t_3} + I_E\\
d_{z_4}\frac{\partial\Theta_4}{\partial t} &= D\left(\frac{\partial\Theta}{\partial z}\right)_{z_3} - D\left(\frac{\partial\Theta}{\partial z}\right)_{z_4} + K_{z_3} - K_{z_4} - E_{t_4}
\end{aligned}
\qquad (2)
$$

where D is hydraulic diffusivity, K is the soil hydraulic conductivity, P_D is precipitation, R is surface runoff and E_{t_i} is the layer root uptake.

The soil was irrigated by adding an extra irrigation term (I_Θ) to the appropriate soil layers. To assess which layers should be irrigated, a site inspection was made, and a lateral distribution radius of 30–40 cm was observed around the pipe. Therefore water was added to the second and third soil layers to approximate this depth and water distribution. The Θ level was replenished every 7 days by the scheme. However, because the whole soil layer was wetted, the drainage over time is very slow, despite uptake and percolation processes, and Θ remains fairly constant over the seven day intervals. The reproduction of soil drainage over time still remains a problem, because in reality the Θ fluctuation would be larger and more rapid from a smaller wetted volume. Therefore,

HESSD
10, 13897–13953, 2013

the variability in canopy ET at short time scales of e.g. a few days, may not be well represented by the model because in reality the soil may dry before the sensors activate new irrigation and higher resistances are likely to occur briefly. In this model simulation therefore, ET is therefore still limited by Θ, but only in terms of the target level applied and not by varying levels of moisture due to drainage/plant uptake, as may happen in reality. Well-reproduced daily variability therefore, might not always be expected but representative diurnal ET magnitudes based on target Θ levels and the environmental conditions are assumed.

4.3 Soils within the plantations

The soils within the plantation are classified as clay loam by the FAO model soil data. Local soil survey data estimates that soils at the plantation are mainly composed of silty to sandy loam, loess soils. These were therefore reclassified to a sandy loam category both in *Impact* and *Control*. Parameters were then refined further using local survey data (see Table 4).

Soil moisture initialisation values appeared to be unrealistically high in the 2nd and 3rd soil layers (see Fig. 7) where Θ fractions of 0.2–0.28 were prevalent, particularly upwind of the plantations and in the desert. These Θ levels approach field capacity for sandy loam soils. Values closer to wilting point are likely to be more realistic during summer after a dry 2012 spring, even at 0.5 m. However, this could not be confirmed as quality data was not available. Nevertheless, if the sub-soil Θ data is unrepresentative, there could be implications for advection of moisture and perhaps the model spin-up time for the soils. The assumption was made that sub-soil Θ from unvegetated surfaces would not be a significant factor due to lack of a transport mechanism from sub-soils to the surface i.e. roots. Of course, there may still be an impact on the thermal diffusion and conductivity of the soil.

The 2nd and 3rd soil layers within the plantation boundary were re-initialised to wilting point (0.047) prior to irrigating. Re-initialising a wider area of soil was considered, but a method for deciding the extent and Θ value was not found.

HESSD
10, 13897–13953, 2013

5 Validation

To judge the model performance and configuration, two cases are assessed. The first is a baseline run with unmodified MODIS land surface data (WRF Control). The second is a simulation of a 10 km × 10 km irrigated plantation (WRF Impact). WRF Control is compared to observations from a desert surface. WRF Impact is compared with observations from Jojoba and Jatropha plantations.

5.1 Comparison with observed quantities

The validation of the Control model run against Desert observations, and Impact against Jojoba are shown in Figs. 8 and 9 as mean diurnal cycles with standard deviations as error bars. It is relevant to compare not only model against observations, but also how the quantities compare between the cases themselves. Note that all times of day discussed represent local summer time (UTC + 4).

T2 (model to observations) – during the daytime, *Desert* T2 values are reproduced extremely well by WRF Control with almost no deviation between 8 a.m. and 9 p.m. The variance is well reproduced throughout the day. After 9 p.m., the model starts to diverge and there is a significant night time cold bias of around 2 °C. A similar overall pattern occurs with WRF Impact which shows a strong cold bias during the night time (up to 5 °C). Here though, the model is also a little too cool during the day (1–1.5 °C). WRF Impact T2 also accurately simulates the variability of Jojoba T2.

T2 (case comparison) – in reality, the observed daytime T2 over Jojoba is warmer than over *Desert* (1 °C) but up to 2 °C cooler during the night (Fig. 8, top panels). If we compare the model's representation of this phenomenon, WRF Impact correctly predicts cooler night time T2 than Control. However, this difference is larger than in reality by some margin (up to 2 °C). WRF Control and Impact have daytime T2 which are almost equivalent, with WRF Impact T2 around 0.5–1 °C cooler than WRF Control.

VPD (model to observations) – WRF Control models the VPD quite accurately throughout the 24 h period including variability, with a maximum bias of +0.2 hPa during

HESSD
10, 13897–13953, 2013

the afternoon when temperatures are highest. WRF Impact also models the VPD relatively well in terms of magnitudes, but exhibits a lag which could lead to a deviation in diurnal ET. The variability is also somewhat over estimated during the mornings.

VPD (case comparison) – during the middle of the day Desert VPD is 0.5 hPa higher than Jojoba. Disregarding the bias itself, WRF models this difference accurately in both magnitude and sign. At night Desert has a slightly higher VPD than Jojoba, reflecting the higher temperatures. Jojoba VPD approaches zero in the morning indicating near-saturated conditions.

U (model to observations) – WRF Control reproduces Desert *U* accurately, exhibiting biases of no more than 0.5 $m s^{-1}$. In fact this bias appears to be one of diurnal phase rather than amplitude, with the WRF Control peak preceding Desert by an hour or so. There is also an unusual *U* peak (0.5–1 $m s^{-1}$) which occurs around 6–7 a.m. in WRF which is not reflected by the observations. The variability is overestimated somewhat (up to 0.5 $m s^{-1}$). Comparing Impact *U* with Jojoba is slightly problematic given the difference in measuring height (6 m) and the model *U* estimation height of 10 m. The WRF Impact *U* peak of 4.5 $m s^{-1}$ is around 1.5 $m s^{-1}$ higher than observed. It is not clear however if all of this difference could simply be attributed to the height discrepancy. Similarly to Control, the WRF Impact peak also appears to precede Jojoba by around 1 h and the variability is slightly overestimated.

U (case comparison) – Desert *U* is considerably more rapid than Jojoba during the middle part of the day (5.5 and 3 $m s^{-1}$ respectively), which is as expected considering the difference in roughness. This is only reproduced partially by WRF – predicting Desert peak *U* to be only 1 $m s^{-1}$ more rapid than Jojoba.

R_n (model to observations) – WRF Control R_n matches closely with Desert observations throughout the day and night with only a deficit of 25 $W m^{-2}$ around midday. WRF Control underestimates the variability a little though during the daytime (around 15 $W m^{-2}$). WRF Impact matches Jojoba somewhat less well with biases of up to 60–70 $W m^{-2}$ (8–10 % of total magnitude), although the variability is simulated accurately.

HESSD
10, 13897–13953, 2013

R_n (case comparison) – during the day, observed Jojoba R_n at 1 p.m. (740 $W m^{-2}$) reaches 300 $W m^{-2}$ higher than Desert. During the night, net losses for Desert and Jojoba are quite similar – between 60 and 100 $W m^{-2}$. WRF models these relative characteristics very closely.

G (model to observations) – WRF Control overestimates *G* during the day from around 10 a.m. onward. This positive bias reaches 30 $W m^{-2}$ at around 12–1 p.m. The variability is also somewhat overestimated. During the night, *G* losses are overestimated – up to 25 $W m^{-2}$ during the late evening. WRF Impact overestimates *G* by up to 20 $W m^{-2}$ during the day and also overestimates the upward night time flux also up to 20 $W m^{-2}$. In both model cases the morning *G* gradient has a slope that is too steep in comparison with the observations. Additionally in both model cases, the model appears to lag the observations (1 and 2 h for Control and Impact, respectively). If these anomalies were corrected, the biases would be considerably reduced over much of the day.

G (case comparison) – as expected, observed peak *G* is considerably higher in the Desert soil than in Jojoba – with a ratio of around 2 : 1. Observed night time *G* losses also hold to this ratio with desert losses larger than Jojoba. Again disregarding the absolute values, WRF reflects this daytime ratio between the surfaces.

ST5 (model to observations) – WRF Control underestimates the 5 cm soil temperatures, although the variability is well simulated. Both cases exhibit a significant cold night time bias, corresponding to the bias in T2. The night time biases approach 4 °C for both cases. During the day WRF Control converges significantly with Desert and is only 1 °C cooler around midday. WRF Impact ST5 exhibits a more damped amplitude than Jojoba and bisects Jojoba at around 3 p.m., then underestimating the peak ST5 by up to 2 °C.

ST5 (case comparison) – Desert ST5 has a much greater amplitude (15 °C) than Jojoba (5 °C). WRF Control predicts an amplitude which is too large (18.5 °C) compared to Desert, likely due to the large night time T2 bias and WRF Impact also overestimates the amplitude by around 4 °C. ST5 drops to around 28 °C at night time whereas Jojoba

HESSD
10, 13897–13953, 2013

drops to around 26.5 °C. Peak ST5 occurs at around 5 p.m. for Desert and around 6 p.m. for Jojoba. These peaks are modelled very well by WRF in both cases.

5.2 Comparison with evapotranspiration estimates

Since measurements of vertical fluxes were not available, ET was calculated independently from WRF-NOAH by applying two formulas based on Penman–Monteith equations (see below) and the observed Jojoba meteorological data. Penman–Monteith methods were thought to be appropriate here because they are often used in conditions where water is not greatly limited, such as with irrigated crops. Estimations in conditions where water stress is present are more problematic and other methods may be more suitable, e.g. parameterized ET sub-models based in hydrologic models (Sumner and Jacobs, 2005). Additional estimates were examined from Becker et al. (2013) and also from a USAID report (Irrigation and Crop Management Plan, 2006) – both of which discuss ET estimates for a Jatropha plantation (Luxor, Egypt) in a similar summer climate (winter is warmer and drier though). Jatropha ET was not estimated because of the small plantation size and the likelihood of biases from advection.

Two methods were used: (a) the combination Penman–Monteith equation (Penman R_a/R_s) and (b) a modified Penman Monteith ASCE method (Penman 56 FAO) (see Appendix B for descriptions). The first method, Penman R_a/R_s is based on the so called combination Penman Monteith equation from Monteith (1965) which includes explicit surface and aerodynamic resistances. The second method, Penman Monteith 56 FAO (Allen, 1998) was developed by the Food and Agriculture Organisation (FAO) – a standard analytic/empirical method, useful when stomatal resistance data are not available. It describes a potential or reference ET (ET_0) of a well-watered vegetated grass surface with canopy height of 0.12 m, a constant Rs of 70 s m^{-1} and an albedo of 0.23. This ET_0 value is then modified with a crop coefficient K_c associated with particular plant types (see 5.1 for a detailed description of both methods and for calculations).

Both methods generally assume a neutrally stable surface layer which, given the dry convective afternoon conditions in hot, arid climates, when thermal turbulence

HESSD
10, 13897–13953, 2013

dominates, is often not the case. Methods have been devised to include stability functions. The MM5 surface layer scheme (see Table 1) selected for the model simulations does employ a stability correction factor (S) which is combined with wind speed to calculate evaporation (see Sect. 5.1.1 for a description). However, it is not completely clear whether the inclusion of stability correction affects ET calculations substantially or not. Mahrt and Ek (1984) in a study based on the Wangara experiment and Otles and Gutowski (2005), from a modelling study in a semi-arid climate, both discuss this issue. They tested methods with and without stability correction, with fairly similar results, both of which matched their lysimeter and flux observations closely. Bearing this in mind and because the absence of profile data makes the stability regime hard to identify, no stability correction was used in this case for estimations.

The mean daytime Jojoba evaporation estimates (averaged for all summer months) from both Penman Monteith methods are shown in Table 5. Both methods yield very similar mean daytime ET_C values (Penman R_a/R_s 4.56 mm d^{-1} and Penman 56 FAO 4.33 mm d^{-1}). The quality of these estimations were assessed through comparison with annual data gathered for the Luxor Jatropha plantation, from the USAID report (also based on the FAO 56 approach). In Luxor, mean Jatropha ET_C values of 4.86 mm d^{-1} are quoted for the summertime (see Fig. 10), which is a very close match. The annual total ET_C in Luxor is estimated to be around 1250 mm. In Israel on the other hand, agronomists quote an annual input of 700 mm for Jojoba (650 mm for Jatropha). The average 200 mm of winter rain in Beer'sheva can be added to that. If the above annual irrigation inputs are accurate, there still remains around a 300 mm difference between the Israel and Egypt totals. This difference may be attributed to (a) cruder, surface irrigation in Luxor, where greater losses to direct evaporation and runoff could be assumed, and also (b) the cooler winter climate in Israel. Therefore, less water is needed in Israel during the winter and 900 mm yr^{-1} may therefore be a plausible water requirement. Additionally, three harvests are obtained every growing season in Luxor which necessitates more irrigation than if only two per year were taken. However, if we

HESSD
10, 13897–13953, 2013

concentrate only on the summer months, where observations for Israel are available, then the Penman estimates match the Luxor ET rates to within 0.5 mm d^{-1}.

ET from the Penman Monteith ET estimates and from the WRF-NOAH model, are compared in Fig. 11 (left panel), and are expressed in both W m^{-2} and mm d^{-1}.

The remainder of the energy balance for these two methods was then estimated from the G and R_n observations. The WRF HFX fluxes were plotted against the plantation HFX values implied by the ET estimations, calculated as the residual of the energy balance (Eq. 3):

$$\mathrm{HFX} = R_n(\mathrm{Obs}) - G(\mathrm{Obs}) - \mathrm{LH}(\mathrm{Estimate}). \quad (3)$$

R_n measurements should be fairly representative, but a good representation of G is difficult to obtain without many measurement points due to: soil heterogeneity, sharp temperature gradients and diurnal changes in shading caused by the partially open Jojoba canopy. Additionally the heat storage needs to be accounted for which requires good estimations of wet/dry soil thermal conductivities and Θ. In spite of these factors, during the middle part of the day, G magnitudes play only a minor role in the energy balance (for Jojoba, 5 % of R_n). Therefore, day time biases in G should not overly affect estimates of the other energy fluxes, based on $R_n - G$. During the night however, biases in G could play a larger role where R_n and G flux magnitudes approach each other.

The resulting Penman ET curves are quite similar in magnitude with a 1 mm d^{-1} or 28 W m^{-2} difference during the middle of the day. The Penman 56 FAO curve shows a slight lag of perhaps 1 h, when compared with Penman R_a/R_s, and has a less peaked shape. At night, Penman 56 FAO exhibits only a very small downward flux (perhaps 5 W m^{-2}), whereas Penman R_a/R_s shows a higher downward flux of 10–20 W m^{-2}. WRF Impact ET matches well in magnitude with the Penman estimates, and during the day the WRF curve falls somewhere between the two Penman curves with a maximum latent heat value of 160–170 W m^{-2}. After sunrise, WRF Impact follows closely with the Penman R_a/R_s ET curve until midday when the model diverges a little. Around 2 p.m., the Penman R_a/R_s curve drops sharply and bisects the WRF curve which predicts high

HESSD
10, 13897–13953, 2013

ET for a longer period before dropping more smoothly downward between 2 and 4 p.m. The peak time (of highest ET) in the model lies in between those from the Penman estimates with all three curves being spaced around 30 min apart. During the latter part of the afternoon and evening, WRF matches more closely with Penman 56 FAO.

For the estimated HFX (Fig. 11, right panel), WRF Control HFX is also plotted alongside WRF Impact and the two Penman estimates. WRF Impact approaches most closely to Penman R_a/R_s in magnitude and shape. What is noticeable is that HFX from both Penman estimates have higher peak magnitudes than WRF Impact, which seems contradictory to what the LH plot implies, where WRF LH falls in between the two estimates. This apparent anomaly can be explained by (a) the slightly lower WRF Impact R_n during the day and (b) the differences of alignment in peaks for observed and modelled R_n and G (Fig. 9). At night time, both Penman estimates exhibit large downward HFX (−50 to −100 $W m^{-2}$) in the late evening which is not reflected by WRF Impact.

A clear finding is that daytime WRF Impact HFX is significantly higher than WRF Control over the area of the plantation (+150 to 160 $W m^{-2}$).

6 Discussion

The aim of the study was to configure and parameterize the WRF-NOAH model for the Eastern Mediterranean region, validate it with observations and then simulate a subsurface irrigated 100 km^2 plantation in south-central Israel. The success of the simulation was examined by: (a) validating WRF Control and Impact T2, Q2, U, R_n, G and ST5 output against the corresponding desert and vegetation observations in terms of mean diurnal cycles, and (b) comparing modelled ET quantities against two Penman–Monteith estimates. Based on the results it was intended to draw conclusions on the:

- model ability to reproduce surface quantities over the desert and vegetation,
- success of model parameterization and potential model improvements,

HESSD
10, 13897–13953, 2013

– comparative fluxes over vegetation and desert.

6.1 Validation results

WRF Impact diagnoses cooler morning and midday temperatures over Jojoba in contrast to WRF Control and Desert (Fig. 8) but it is not clear why this is so. T2 measurement error is likely to be negligible (see Table 1). One possibility is that the larger Impact night time cold bias is extended into the convective ABL. Another possible cause is the lag in R_n, exhibited by WRF Impact during this period. Other possibilities are advection effects over the plantations due to the disparity in simulated and real plantation sizes. This scale effect needs to be tested with different simulated plantation sizes in further studies.

The night time T2 cold bias is large and is reflected in 5 cm soil and skin temperatures which are too cold (and upwelling long wave flux which is too low). This could be due to difficulties in the model simulation of the stable boundary layer and during ABL regime transitions. However, this evaluation being more concerned with daytime ABL evolution, will focus mainly on the daytime simulation results as a priority.

VPD is simulated reasonably accurately (deviation < 1 hPa) indicating that at least in terms of potential evaporation, the model simulates climatic evaporative demand closely (see Appendix A for NOAH evaporation mechanism). How this relates in reality to bulk surface resistances and ET_C for Jojoba over the day is not so clear. Under constant light and VPD, the stomatal aperture of Jojoba is controlled by the xylem water potential (ψ) of the plant. Furthermore the plant responses to changes in ψ are heavily dependent on soil and air temperatures and are therefore highly non-linear (Benzioni and Dunstone, 1988).

U is of great importance to the estimation of energy balance partitioning given the influence on turbulent exchanges. It is well modelled over the desert surface but over the plantation the observed surface winds are $1.5\,m\,s^{-1}$ slower than the model. As mentioned, this could be explained partly by the disparity in model and observation heights, but it is difficult to say to what degree. Other possibilities include local complexities in

HESSD
10, 13897–13953, 2013

the turbulent wind field being introduced by the broken canopy. Finnegan et al. (2009) found that pressure gradients between the front and back side of leaves and stems lead to unique turbulent characteristics in the roughness sub-layer and suggest that Monin Obhukov assumptions (as made in the MM5 surface layer scheme) are not necessarily valid over canopies. In spite of this, the tentative assumption may be risked that at least the U curves would be closer in magnitude, had the observations been obtained at 10 m.

R_n is very well modelled for both Control and Impact for the majority of the day (Fig. 9). There is a slight underestimation for both cases around peak time (2 p.m.) of 30–50 W m^{-2}. This could be explained by a lower atmosphere in the model which is too dry, resulting in a reduced downwelling of long wave (LW) radiation. The LW component was investigated for both cases and a deficit does indeed exist which accounts for nearly all of the reduced R_n. However, given that this anomaly represents only a small fraction of the R_n magnitude, this bias should not overly compromise energy balance estimates.

G is not well represented by the model in the desert by WRF Control, being overestimated by around 30 % but Jojoba G is better modelled by WRF Impact. In both cases the morning upward slope is too sharp in the model, especially in Control. This could indicate: (a) a temperature gradient that is too large between the skin and soil, (b) misparameterized thermal conductivity, dependent on Θ described in Chen and Dudhia (2001), or (c) misclassified soil texture/characteristics. It is also possible that there are measurement errors in the desert site due to soil heterogeneity or due to large temperature gradients. However, there is a very high correlation between the two desert flux plates over the summer time series (0.99) which more or less rules out relative errors between the two plates. The temperature measurements could be prone to error though due to the singular measurement. The overall contribution of observed G to the energy balance is not very large in the plantation (5–6 %), but it is larger in the desert (20 %). In the desert, where there is little ET any bias in G will inevitably affect HFX exclusively. If the measurements are in fact representative, then WRF Control is

HESSD
10, 13897–13953, 2013

overestimating G, and underestimating HFX by around 30 W m^{-2} at peak time. This needs to be accounted for when comparing fluxes.

The ST5 validation again reflects the night time cold bias already discussed both in WRF Control and Impact. However the bias is strongest in Control. Some of this difference can be explained by the greater upward night time G in Control (20 W m^{-2}) than from the plantation soils (10–12 W m^{-2}). During the daytime the model converges with the observations. This could be explained by the steeper model slope which allows the model to make up the deficit from the night time somewhat.

6.2 Diurnal energy fluxes

In terms of predicting peak ET magnitudes, the model agrees largely with the Penman estimates, and lies within 20 W m^{-2} of both curves at peak time (Fig. 11, left panel). Both the shape and the magnitude of WRF Impact appears to fall in the middle Penman R_a/R_s and 56 FAO. If we can assume that the Penman methods are valid, this lends confidence to the simulated peak LH of 160 W m^{-2}. Extrapolating these flux estimates to HFX, the evidence suggests that a surplus of around 120–130 W m^{-2} (Fig. 11, right panel) exists between the irrigated Jojoba and desert surfaces (90–100 W m^{-2} if we allow for the 30 W m^{-2} G overestimation by WRF Control). Therefore it is likely that a strong horizontal HFX gradient would develop if large plantations are implemented in a hot desert.

7 Conclusions and outlook

The first aim of the study was to configure and parameterize the WRF-NOAH model for an arid region such that the model can simulate daytime surface quantities which dictate the energy balance, over bare soils and over irrigated vegetation surfaces. This has to a large degree been successful in terms of magnitude and variability. If we consider the daytime model performance, deviations are evident (slightly more so over

HESSD
10, 13897–13953, 2013

the vegetated surface), but do not appear significant enough to invalidate further impact studies of e.g. plantation scale on ABL evolution. Unfortunately, for reasons unknown, the night time performance of this configuration of WRF-NOAH is still poor for some processes but an investigation on this topic is out of the scope of this study.

Further calibration with sensitivity tests could further improve the LSM model for local conditions. One evident weakness is the simulation of soil thermal transport, especially in the desert soils (if we assume that the fault lies with the model and not the G and ST5 observations). Confidence in the model is reinforced by the close match of simulated ET both with the two Penman–Monteith estimation methods and with the summer data from Luxor. This is of course assuming that the Penman–Monteith methods used are valid in arid conditions and for desert plants such as Jojoba or Jatropha. Vertical flux, profile and soil/plant measurements are planned in the future for the Jojoba, to further investigate the efficacy of the Penman methods used and to provide further calibration and information on stability.

In the context of our assumptions, the prediction can be made that sensible heat fluxes (HFX) over the plantations can be higher than over desert surfaces, mainly due to the large difference in R_n and lower ET from well-adapted desert species, relative to freely transpiring canopies. These predictions of large plantation T2 and HFX magnitudes appear to differ with conclusions from regional irrigation impact studies (e.g. Qian et al., 2013; Kueppers et al., 2007) which diagnose cooler (daily mean) T2 and lower Bowen ratios over irrigated plantations. This has significant implications, not least for possible impacts on local and regional climate if larger scale biomass plantations are planned.

HESSD
10, 13897–13953, 2013

Appendix A

NOAH LSM ET_C

The following expression based on a Penman Monteith formulation is used by NOAH to calculate ET_C (see e.g. Chen and Dudhia, 2001) (Eq. A1).

$$ET_C = \underbrace{\left(\frac{\Delta(R_n - G)}{L_v(\Delta + 1)} + \frac{\rho_a(e_s - e_a)}{S(1+\Delta)}\right)}_{\text{Potential ET}} \left[\underbrace{(1-\sigma_f)\frac{\Theta - \Theta_w}{\Theta_{FC} - \Theta_w}}_{\text{Direct ET}} + \sigma_f \left(\underbrace{\left[\frac{W_C}{\mu}\right]^{0.5}}_{\text{Wet Canopy ET}} + \left[\underbrace{1 - \left(\left[\frac{W_C}{\mu}\right]^{0.5}\right) B_C}_{\text{Dry Canopy ET}}\right]\right)\right] \quad \text{(A1)}$$

where $R_n - G$ is the available radiation ($MJ\,d^{-1}$), Δ is the slope of saturation vapour pressure against temperature, L_v is the latent heat of vaporization ($J\,kg^{-1}$), ρ_a is surface air density ($kg\,m^{-3}$), $e_s - e_a$ is the VPD (kPa), S is a stability coefficient and represents C_qU, where C_q is the turbulent exchange coefficient for water vapor, described by the Richardson number. Θ_{FC} is the field capacity and Θ_w is the wilting point. W_C is the intercepted canopy water content ($kg\,m^{-2}$), μ is the maximum canopy capacity ($kg\,m^{-2}$) and B_C is a modifier, analogous to K_C in Penman 56 FAO, used to calculate ET_C from ET_O (Eq. A2):

$$B_C = \frac{1 + \frac{\Delta}{R_r}}{1 + R_c C_q + \frac{\Delta}{R_r}}. \quad \text{(A2)}$$

HESSD
10, 13897–13953, 2013

$R_r = f(U,T,P,C_h)$, and R_c is the canopy resistance. For R_c NOAH uses the Jarvis type scheme, also described in Chen and Dudhia (2001), for calculating R_C (Eq. A3):

$$R_c = \frac{R_{c\,min}}{LAI_{eff} F1 F2 F3 F4} \quad \text{(A3)}$$

where $R_{c\,min}$ is an empirical constant and LAI_{eff} is the effective leaf area index (generally $0.5 \times LAI$). $F1$, $F2$, $F3$, $F4$ are coefficients representing the effect of radiation, air humidity, air temperature and soil moisture on R_c, respectively. $F3$, the temperature coefficient is given by $1 - 0.0016(T_{ref} - T)^2$ where T_{ref} is an optimum temperature for maximum photosynthesis and $F4$, the soil moisture factor is given by the layer discretized expression (Eq. A4):

$$F4 = \sum_{i=1}^{nroot} \frac{\Theta - \Theta_w}{\Theta_{FC} - \Theta_w} f_{root} \quad \text{(A4)}$$

where nroot is the number of soil layers where roots are present and f_{root} is the layer's fraction of the root zone.

Appendix B

Field ET estimation methods

There are standard methods used to estimate ET from vegetated surfaces, including so called Penman–Monteith methods (Penman, 1948; Monteith, 1965). Since Penman developed a method to estimate ET from an open water surface, others included evaporation estimates from other surfaces like canopies, by incorporating various resistance terms. Further research includes the effects of different stability regimes – for instance, Mahrt and Ek (1984) and Otles and Gutowski (2005). Different methods have been devised and are used depending on (a) data availability, (b) required interval for averaging e.g. daily/hourly; and (c) what assumptions can be made e.g. stability.

HESSD
10, 13897–13953, 2013

Penman–Monteith R_a/R_s equation (Monteith, 1965)

The following expression is the Penman Monteith (Penman R_a/R_s) equation formulated to account for explicit surfaces and aerodynamic resistances (Eq. B1):

$$ET_C = \frac{\Delta(R_n - G)}{L_v(\Delta + 1)} + \frac{\rho_a C_p \frac{(e_s - e_a)}{R_a}}{\Delta + \gamma\left(1 + \frac{R_s}{R_a}\right)} \quad \text{(B1)}$$

where ET_C is the crop ET ($mm\,d^{-1}$), C_p is the specific heat of air at constant pressure ($J\,K\,g^{-1}\,K^{-1}$, γ is the psychrometric constant [$kPa\,K^{-1}$], R_s and R_a are the surface and aerodynamic resistances respectively ($s\,m^{-1}$). The resistance terms are defined respectively as (Eqs. B2 and B3):

$$R_s = \frac{R_l}{LAI_{eff}} \quad \text{(B2)}$$

$$R_a = \frac{\ln\left(\frac{Z-d}{Z_{0m}}\right)\ln\left(\frac{Z-d}{Z_{0h}}\right)}{k^2 U_z} \quad \text{(B3)}$$

where R_l represents the bulk stomatal resistance. In the second expression, Z is the standard measurement height, Z_{0m} is the roughness height for momentum, d is the displacement height, Z_{0h} is the roughness height for water vapor and k is von Karman's contant. Estimations for d, Z_{0m}, Z_{0m} have been suggested (Allen, 1998), assuming that roughness heights for vapour and heat are equivalent (Eqs. B4–B6):

$$d = 2/3h \quad \text{(B4)}$$

$$Z_{0m} = 0.123h \quad \text{(B5)}$$

$$Z_{0h} = 0.1Z_{0m} \quad \text{(B6)}$$

HESSD
10, 13897–13953, 2013

where h is the height of the canopy. In order to use this method, values for bulk stomatal resistances (R_l) are a prerequisite. Estimations for Jojoba resistances under different conditions were collated for the report of the Seventh Conference on Jojoba (1988) and are shown in Table B1.

From these estimates it can be deduced that mean R_l values of between 300 and 650 seem feasible for well watered plants in summertime. The difference in early morning resistance (250 s m^{-1}) compared to 11 a.m. (500 s m^{-1}) reflects a common desert plant strategy of closing the stomata during the hotter parts of the day. Another factor when choosing a suitable R_l value is that in reality, although the plants are watered adequately, only the minimum amount needed for plant health and optimized yields, are fed to the plants. In arid regions, even with slightly compromised yields, Jojoba production could still be optimal if the savings in water costs exceed the opportunity costs conceded due to lower yields. Lower inputs would indicate higher R_l values. In other words, under greater water stress it is reasonable to expect higher values of R_l. Regarding the effect of salinity on stomatal resistance, extremely high R_l values are estimated for salt-sensitive plants in saline soils, even exceeding 1000 s m^{-1}.Given the mean values of 1 dS m^{-1} quoted for the irrigation water it is likely that only a minimum of leaching by winter rains may be needed to avoid salt accumulation. The FAO (Ayers and Westcott, 1985) quote one method for estimating the annual water requirement for leaching as $A_w = ET(1 - LR)$, where A_w is the annual water requirement including irrigation and ET is the annual irrigation applied. LR is a coefficient for the minimum leaching requirement needed to control salts within the tolerance of the crop. This is calculated as $LR = EC_w/(5EC_e - EC_w)$, where EC_w is the salinity of the applied irrigation water in dS m^{-1}. EC_e is the average soil salinity tolerated by the crop as measured on a soil saturation extract. The FAO recommends that the tolerance value used should represent a maximum of 90 % reduction of the potential yield, but 100 % for moderate to heavy salinity (> 1.5 dS m^{-1}). Only sparse data on Jojoba salt tolerance is available and many factors could complicate estimates, such as plant varieties and age. Hussein et al. (2011) reported that young Jojoba plants can withstand up to 8 dS m^{-1}, with

HESSD
10, 13897–13953, 2013

one variety "Siloh" tolerating 10 $dS\,m^{-1}$ with no reduction in flower production. However these are juvenile plants or seedlings. They also state that salt tolerance increases with the age and vigour of the plants. If we insert a value of 8 $dS\,m^{-1}$ and an annual ET of 700 mm for Jojoba, this yields a leaching requirement of 20 mm. If we are more conservative and choose a tolerance of 2 $dS\,m^{-1}$ (as estimated in Ayers and Westcott, 1985, for sorghum, grapefruit and orange trees), and assuming a maximum 10 % yield reduction this would require around 90 mm. Therefore, it is safe to assume that any accumulated salt is leached by the 200 mm of winter rain which is average for Beer'sheva. Anecdotally, the managers report that there has been no significant soil degradation due to salinization, even dating back to 1948 when the first plantations were implemented. In spite of this, it is apparent that at least some salt is present in the soils during summer, and this is evident from small patches of salt accruing where water has occasionally breached the surface. Given the very high sensitivity of Jojoba stomatal resistance to salt stress (Table B1), it was thought to be safer to assume a small amount of salt stress. Therefore, a corresponding value of 800 $s\,m^{-1}$ was estimated for R_l. This higher value can also be justified by the deficit irrigation technique which is associated with higher resistances when compared with cruder methods e.g. surface irrigation. In this regard, stomatal resistances could also exhibit a diurnal peak during the afternoon when soil water around the roots becomes depleted, and soil water is redistributed at night.

Mean seasonal hourly values calculated from this Penman method were multiplied by the vegetated fraction (σ_f) estimated at 70 %.

HESSD
10, 13897–13953, 2013

Penman 56 FAO Equation (Allen, 1998)

The following expression is the Penman Monteith equation (Penman 56 FAO) using a crop coefficient K_c to modify ET_o (Eq. B7):

$$ET_o = \frac{0.408\Delta(R_n - G) + \gamma\left(\frac{900\,(K)}{T\,(^\circ C)+273.16}\right)\frac{u_z\,(m\,s^{-1})}{m\,s^{-1}}(e_s - e_a)}{\Delta + \gamma(0.34u_z\,(m\,s^{-1}) + 1\,m\,s^{-1})} \quad \text{(B7)}$$

where ET_o is the potential evapotranspiration ($mm\,d^{-1}$), $R_n - G$ is the net available radiation ($MJ\,d^{-1}$), T is temperature at standard height (°C) and u_z is the wind speed at standard height ($m\,s^{-1}$). ET_c is modified using K_C i.e. $ET_c = ET_o \times \sigma_f \times K_c$, where ET_c represents the actual crop ET estimate. In general terms the ET_o can be thought of as the first-order climatic demand and K_C is a modifier. K_C accounts for species specific physiological and physical factors, differentiating the crop from the reference vegetation and is intended to represent the effect of: crop type, albedo, stomatal resistance and direct soil evaporation. It is the ratio of ET_o to the ET_c and is often < 1, but not in all cases. With closely spaced tall freely transpiring canopies, K_C can be as much as 15 to 20 % > 1. A dual K_C method can also be used by splitting the coefficient K_C into basal crop and soil evaporation components ($K_{CB} + K_E$). However, since we assume negligible soil evaporation with sub-surface irrigation, K_E would be negligible. We therefore concentrate on the basal effect only i.e. a single K_C value. Normally K_C values are available in lookup tables made available by the FAO but specific values for Jatropha and Jojoba are not given, so values were substituted from the nearest crop type in terms of height, biomass, geographical distribution and characteristics (oil seed crops and fruit tree categories). The validity of doing this is of course debateable. For nearly the whole year, a value of 0.7 is estimated by the FAO for these categories (this falls fractionally to 0.65 in the coolest winter months). Another source gives Jojoba a value of 0.5 all year round (Benzioni and Dunstone, 1998). A constant value is a reasonable assumption in arid regions, especially for the Israel Jojoba plants because they are

HESSD
10, 13897–13953, 2013

fully mature perennials i.e. no more substantial growth, and high radiation all year. This contrasts with some crops such as annuals whose K_C varies widely over phenological stages.

It should be noted that when conditions are calm and humid, the aerodynamic factors of tall, dense canopies have less effect on the ET_o/ET_c ratio than the radiation which is the dominating driver of ET at low wind speeds. When relative humidities are lower than 45 % (assumed in the reference K_C estimates) the vapour pressure deficit (VPD) is higher, and the aerodynamics of taller crops has more effect. This can be better seen from the ratio $(e_s - e_a)R_a{}^{-1}$ in the numerator of Penman, R_a/R_s (Eq. B1). In arid conditions when the VPD is high, the ratio will be larger, which means that a significant change in R_a will have a large effect on the ET_o. Accordingly, the differences in ET_o estimation would be amplified with tall crops experiencing higher wind speeds because the aerodynamic term is proportional to U_z and canopy height. Over the plantations, mean minimum daytime RH values are 29.6 % over the Jatropha and 30.0 % over the Jojoba which represents a large VPD. However the mean daytime wind speeds are low (1.71 ms^{-1} Jatropha and 1.88 ms^{-1} Jojoba) which would likely be a compensating factor. This was checked by using an adjustment modifier for mid-season K_C from Allen, (1998) (Eq. B8):

$$K_C = K_C(\text{Table}) + \left[0.04\left(\frac{\overline{u_Z}(ms^{-1}) - 2ms^{-1}}{ms^{-1}}\right) - 0.004\left(\frac{RH_{min} - 45\%}{\%}\right)\left(\frac{h}{3m}\right)^{0.3}\right] \quad \text{(B8)}$$

where $\overline{u_Z}$ is the mean 2 m daytime wind speed (ms^{-1}) and RH is the minimum daytime relative humidity (%). Using this correction and the observation data, the K_C value remains virtually unchanged because the low RH is offset by low wind speeds. Therefore the K_C values used were not changed for the calculations.

There are other factors which may affect ET, such as crop and leaf geometry to name just two examples. Regarding geometry, in Jojoba the leaf orientation is almost vertical which, as well as affecting the turbulent wind characteristics, would also reduce incident solar radiation on the leaves when the solar zenith angle is low and temperatures

HESSD
10, 13897–13953, 2013

are at their highest. Transpiration and photosynthesis rates tend to be correlated with solar radiation intensity. This would therefore minimize evaporation and heat loading at midday and optimize photosynthesis, when heat and water potential losses are low (Seventh International Conference on Jojoba and Its Uses: Proceedings, 1988). Factors such as these are difficult to take into account within a general K_C coefficient however but further research to improve species specific estimates are out of the scope of this study.

Acknowledgements. The authors thank their colleagues H.S. Bauer, J. Milovac, T. Schwitalla, H.D. Wizemann, A. Behrendt, A. Geissler for continuing support and discussion.

A special thank you to Dan Yakir at the Department of Environmental Sciences and Energy Research, Weizmann Institute of Science, Rehovot, Israel for his valuable scientific contributions and support.

With thanks to the personnel at Kibbutz Hatzerim and NETAFIM, Israel for their continuing technical support with our measurement campaign. Especially, Ami Charitan, Ronen Rothschild, Oscar Lutenberg and Eli Matan.

Many thanks for the support from the High Performance Computing Center Stuttgart (HLRS) of the University of Stuttgart, Germany, where the simulations and analysis were performed on the CRAY XE6 sytem.

References

Abou Kheira, A. and Atta, N.: Response of *Jatropha curcas* L. to water deficits: yield, water use efficiency and oilseed characteristics, Biomass Bioenerg., 33, 1343–1350, 2009.

Allen, R., Pereira, L., Raes, D., and Allen, M.: Crop Evapotranspiration: Guidelines for Computing Crop Water Requirements, FAO Irrigation and Drainage Paper No. 56, Food and Agricultural Organization, Rome, 1998.

Alpert, P. and Mandel, M.: Wind variability – an indicator for a mesoclimatic change in Israel, J. Clim. Appl. Meteorol., 25, 1568–1576, doi:10.1175/1520–0450(1986)025<1568:WVIFAM>2.0.CO;2, 1986.

HESSD

10, 13897–13953, 2013

Ayers, R. S. and Westcot, D. W.: Water Quality For Agriculture, available at: http://www.cabdirect.org/abstracts/19856755033.html;jsessionid=08B1B6FB48B32C38E2994EEEC7EFB14E?freeview=true (last access: 23 September 2013), 1985.
Bauer, H.-S., Weusthoff, T., Dorninger, M., Wulfmeyer, V., Schwitalla, T., Gorgas, T., Arpagaus, M., and Warrach-Sagi, K.: Predictive skill of a subset of models participating in D-PHASE in the COPS region, Q. J. Roy. Meteorol. Soc., 137, 287–305, doi:10.1002/qj.715, 2011.
Becker, K., Wulfmeyer, V., Berger, T., Gebel, J., and Münch, W.: Carbon farming in hot, dry coastal areas: an option for climate change mitigation, Earth Syst. Dynam., 4, 237–251, doi:10.5194/esd-4-237-2013, 2013.
Beljaars, A. C. M.: The parametrization of surface fluxes in large-scale models under free convection, Q. J. Roy. Meteorol. Soc., 121, 255–270, doi:10.1002/qj.49712152203, 1995.
Ben-Gai, T., Bitan, A., Manes, A., and Alpert, P.: Long-term change in October rainfall patterns in southern Israel, Theor. Appl. Climatol., 46, 209–217, 1993.
Ben-Gai, T., Bitan, A., Manes, A., and Alpert, P.: Long-term changes in annual rainfall patterns in southern Israel, Theor. Appl. Climatol., 49, 59–67, doi:10.1007/BF00868190, 1994.
Ben-Gai, T., Bitan, A., Manes, A., and Alpert, P., and Rubin, S.: Spatial and temporal changes in rainfall frequency distribution patterns in Israel, Theor. Appl. Climatol., 61, 177–190, doi:10.1007/s007040050062, 1998.
Benzioni, A.: Jojoba Domestication and Commercialization in Israel, in: Horticultural Reviews, Volume 17, edited by: Janick, J., John Wiley & Sons, Inc., Oxford, UK, doi:10.1002/9780470650585.ch7, 2010.
Benzioni, A. and Dunstone, R. L.: Effect of air and soil temperature on water balance of jojoba growing under controlled conditions, Physiol. Plantarum, 74, 107–112, doi:10.1111/j.1399-3054.1988.tb04949.x, 1988.
Beringer, T., Lucht, W., and Schaphoff, S.: Bioenergy production potential of global biomass plantations under environmental and agricultural constraints, Global Change Biol. Bioenerg., 3, 299–312, doi:10.1111/j.1757-1707.2010.01088.x, 2011.
Chen, F. and Dudhia, J.: Coupling an advanced land surface–hydrology model with the Penn State–NCAR MM5 modeling system, Part I: Model implementation and sensitivity, Mon. Weather Rev., 129, 569–585, doi:10.1175/1520-0493(2001)129<0587:CAALSH>2.0.CO;2, 2001.

HESSD
10, 13897–13953, 2013

Choudhury, B. J. and DiGirolamo, N. E.: A biophysical process-based estimate of global land surface evaporation using satellite and ancillary data I. Model description and comparison with observations, J. Hydrol., 205, 164–185, 1998.
Dalu, G. A., Pielke, R. A., Baldi, M., and Zeng, X.: Heat and momentum fluxes induced by thermal inhomogeneities with and without large-scale flow, J. Atmos. Sci.., 53, 3286–3302, 1996.
Du, C., Wu, W., Liu, X., and Gao, W.: Simulation of soil moisture and its variability in east asia, in: Soc Photo-Opt Instru (SPIE) Conference Series, 62982F-62982F-6, edited by: Gao, W. and Ustin, S. L., International Society for Optics and Photonics, San Diego, California, USA, 2006.
Dyer, A. J. and Hicks, B. B.: Flux-gradient relationships in the constant flux layer, Q. J. Roy. Meteorol. Soc., 96, 715–721, doi:10.1002/qj.49709641012, 1970.
Finnigan, J. J., Shaw, R. H., and Patton, E. G.: Turbulence structure above a vegetation canopy, J. Fluid. Mech., 637, 387–424, 2009.
Fritzmann, C., Löwenberg, J., Wintgens, T., and Melin, T.: State-of-the-art of reverse osmosis desalination, Desalination, 216, 1–76, doi:10.1016/j.desal.2006.12.009, 2007.
Giles, B. D.: Desert Meteorology, Int. J. Climatol., 26, 1737–1738, doi:10.1002/joc.1347, 2006.
Hamilton, A. J., Stagnitti, F., Xiong, X., Kreidl, S. L., Benke, K. K., and Maher, P.: Wastewater Irrigation: The State of Play, Vadose Zone J., 6, 823–840, 2007.
Hong, S.-Y., Noh, Y., and Dudhia, J.: A new vertical diffusion package with an explicit treatment of entrainment processes, Mon. Weather Rev., 134, 2318–2341, doi:10.1175/MWR3199.1, 2006.
Hong, X.: Role of vegetation in generation of mesoscale circulation, Atmos. Environ., 29, 2163–2176, 1995.
Hussain, G., Bashir, M. A., and Ahmad, M.: Brackish water impact on growth of jojoba (*Simmondsia chinensis*), J. Agr. Res., 49, 591–596, 2011.
Khawaji, A. D., Kutubkhanah, I. K., and Wie, J.-M.: Advances in seawater desalination technologies, Desalination, 221, 47–69, doi:10.1016/j.desal.2007.01.067, 2008.
Kueppers, L. M., Snyder, M. A., and Sloan, L. C.: Irrigation cooling effect: regional climate forcing by land-use change, Geophys Res. Lett., 34, L03703, doi:10.1029/2006GL028679, 2007.

HESSD
10, 13897–13953, 2013

Letzel, M. and Raasch, S.: Large eddy simulation of thermally induced oscillations in the convective boundary layer, J. Atmos. Sci., 60, 2328–2341, doi:10.1175/1520-0469(2003)060<2328:LESOTI>2.0.CO;2, 2003.
Mahfouf, J. F., Evelyne, R., and Mascart, P.: The influence of soil and vegetation on the development of mesoscale circulations, J. Appl. Meteorol., 26, 1483–1495, 1987.
Mahrt, L. and Ek, M.: The influence of atmospheric stability on potential evaporation, J. Clim. Appl. Meteorol., 23, 222–234, 1984.
Mlawer, E. J., Taubman, S. J., Brown, P. D., Iacono, M. J., and Clough, S. A.: Radiative transfer for inhomogeneous atmospheres: RRTM, a validated correlated-k model for the longwave, J. Geophys. Res., 102, 16663–16682, 1997.
Monteith, J.: Evaporation and environment, Symp. Soc. Exp. Biol., 19, 205–234, 1965.
Morrison, H. and Gettelman, A.: A new two-moment bulk stratiform cloud microphysics scheme in the Community Atmosphere Model, Version 3 (CAM3), Part I: Description and numerical tests, J. Climate, 21, 3642–3659, doi:10.1175/2008JCLI2105.1, 2008.
Oron, G., Campos, C., Gillerman, L., and Salgot, M.: Wastewater treatment, renovation and reuse for agricultural irrigation in small communities, Agr. Water Manage., 38, 223–234, doi:10.1016/S0378-3774(98)00066-3, 1999.
Otles, Z. and Gutowski, W. J.: Atmospheric stability effects on Penman–Monteith evapotranspiration estimates, Pure Appl. Geophys., 162, 2239–2254, doi:10.1007/s00024-005-2713-8, 2005.
Otterman, J.: Enhancement of surface–atmosphere fluxes by desert-fringe vegetation through reduction of surface albedo and of soil heat flux, Theor. Appl. Climatol., 40, 67–79, 1989.
Otterman, J., Manes, A., Rubin, S., Alpert, P., and Starr, D. O.: An increase of early rains in Southern Israel following land-use change?, Bound.-Lay. Meteorol., 53, 333–351, doi:10.1007/BF02186093, 1990.
Paulson, C. A.: The mathematical representation of wind speed and temperature profiles in the unstable atmospheric surface layer, J. Appl. Meteorol., 9, 857–861, doi:10.1175/1520-0450(1970)009<0857:TMROWS>2.0.CO;2, 1970.
Penman, H. L.: Natural evaporation from open water, bare soil and grass, P. Roy. Soc. A-Math. Phy., 193, 120–145, 1948.
Perlin, N. and Alpert, P.: Effects of land use modification on potential increase of convection: a numerical mesoscale study over south Israel, J. Geophys. Res., 106, 22621–22634, 2001.

HESSD
10, 13897–13953, 2013

Qian, Y., Huang, M., Yang, B., and Berg, L. K.: A modeling study of irrigation effects on surface fluxes and land–air–cloud interactions in the Southern Great Plains, J. Hydrometeorol., 14, 700–721, doi:10.1175/JHM-D-12-0134.1, 2013.

Rajaona, A. M., Brueck, H., Seckinger, C., and Asch, F.: Effect of salinity on canopy water vapor conductance of young and 3-year old *Jatropha curcas* L., J. Arid. Environ., 87, 35–41, 2012.

Ridder, K. and De Gallée, H.: Land surface-induced regional climate change in southern Israel, J. Appl. Meteorol., 1993, 1470–1485, doi:10.1175/1520-0450(1998)037<1470:LSIRCC>2.0.CO;2, 1998.

Rotach, M. W., Ambrosetti, P., Apenzeller, C., Arpagus, M., Fontannaz, L., Fundel, F., Germann, U., Hering, A., Liniger, M. A., Stoll, M., Walser, A., Bauer, H.-S., Behrendt, A., Wulfmeyer, V., Bouttier, F., Seity, Y., Buzzi, A., Davolio, S., Carazza, M., Denhard, M., Dorniger, M., Gorgas, T., Frick, J., Hegg, C., Zappa, M., Keil, C., Volkert, H., Marsigli, C., Montaini, A., McTaggart-Cowan, R., Mylne, Kl., Ranzi, R., Richard, E., Rossa, A., Santos-Muñoz, D., Schär, C., Staudinger, M., Wang, Y., and Werhan, J.: MAP D-PHASE: Realtime Demonstration on Weather Forecast Quality in the Alpine Region, B. Am. Meteorol. Soc., 90, 1321–1336, 2009.

Rotach, M. W., Ambrosetti, P., Apenzeller, C., Arpagus, M., Fontannaz, L., Fundel, F., Germann, U., Hering, A., Liniger, M. A., Stoll, M., Walser, A., Bauer, H.-S., Behrendt, A., Wulfmeyer, V., Bouttier, F., Seity, Y., Buzzi, A., Davolio, S., Carazza, M., Denhard, M., Dorniger, M., Gorgas, T., Frick, J., Hegg, C., Zappa, M., Keil, C., Volkert, H., Marsigli, C., Montaini, A., McTaggart-Cowan, R., Mylne, Kl., Ranzi, R., Richard, E., Rossa, A., Santos-Muñoz, D., Schär, C., Staudinger, M., Wang, Y., and Werhan, J.: MAP D-PHASE: Realtime Demonstration on Weather Forecast Quality in the Alpine Region, B. Am. Meteorol. Soc., 90, 1321–1336, 2010.

Rotenberg, E. and Yakir, D.: Contribution of semi-arid forests to the climate system, Science, 327, 451–454, 2010.

Schwitalla, T., Bauer, H.-S., Wulfmeyer, V., and Zängl, G.: Systematic errors of QPF in low-mountain regions as revealed by MM5 simulations, Meteorol. Z., 17, 903–919, 2008.

Seventh International Conference on Jojoba and its Uses: Proceedings: The American Oil Chemists Society, available at: http://books.google.com/books?id=gLSt4EiTYzgC&pgis=1 (last access: 5 March 2013), 1988.

HESSD
10, 13897–13953, 2013

Silva, E. N., Ribeiro, R. V., Ferreira-Silva, S. L., Viégas, R. A., and Silveira, J. A. G.: Comparative effects of salinity and water stress on photosynthesis, water relations and growth of *Jatropha curcas* plants, J. Arid. Environ., 74, 1130–1137, 2010.

Skamarock, W., Klemp, J. B., Dudhia, J., Gill, D. O., Barker, D., Duda, M. G., Huang, X.-Y., and Wang, W.: A Description of the Advanced Research WRF Version 3, available at: http://opensky.library.ucar.edu/collections/TECH-NOTE-000-000-000-855, last access: 14 November 2013, doi:10.5065/D68S4MVH, 2008.

Spreer, W., Nagle, M., Neidhart, S., Carle, R., Ongprasert, S., Müller, J., and Muller, J.: Effect of regulated deficit irrigation and partial rootzone drying on the quality of mango fruits (*Mangifera indica* L., cv. "Chok Anan"). Agr. Water Manage., 88, 173–180, 2007.

Sumner, D. M. and Jacobs, J. M.: Utility of Penman–Monteith, Priestley–Taylor, reference evapotranspiration, and pan evaporation methods to estimate pasture evapotranspiration, J. Hydrol., 308, 81–104, doi:10.1016/j.jhydrol.2004.10.023, 2005.

United States Agency for International Development (USAID) and Ministry of State for Environmental Affairs Egyptian Environmental Affairs Agency: Irrigation and Crop Management Plan, available at: http://www.mwri.gov.eg/project/report/IWRMI/Report25Task6IrrigationandCropManagmentPlan.pdf (last access: 18 September 2013), 2006.

Van Heerwaarden, C. C., Vilà-Guerau de Arellano, J., Moene, A. F., and Holtslag, A. A. M.: Interactions between dry-air entrainment, surface evaporation and convective boundary-layer development, Q. J. Roy. Meteorol. Soc., 135, 1277–1291, doi:10.1002/qj.431, 2009.

Webb, E. K.: Profile relationships: the log-linear range, and extension to strong stability, Q. J. Roy. Meteorol. Soc., 96, 67–90, doi:10.1002/qj.49709640708, 1970.

Weusthoff, T., Ament, F., Arpagaus, M., and Rotach, M. W.: Assessing the benefits of convection-permitting models by neighborhood verification: examples from MAP D-PHASE, Mon. Weather Rev., 138, 3418–3433, doi:10.1175/2010MWR3380.1, 2010.

Wulfmeyer, V., Behrendt, A., Bauer, H.-S., Kottmeier, C., Corsmeier, U., Blyth, A., Craig, G., Schumann, U., Hagen, M., Crewell, S., Di Girolamo, P., Flamant, C., Miller, M., Montani, A., Mobbs, S., Richard, E. Rotach, M. W., Arpagaus, M., Russchenberg, H., Schlüssel, P., König, M., Gärtner, V., Steinacker, R., Dorninger, M., Turner, D. D., Weckwerth, T., Hense, A., and Simmer, C.: The Convective and Orographically-induced Precipitation Study: a research and development project of the World Weather Research Program for improving quantitative

HESSD
10, 13897–13953, 2013

precipitation forecasting in low-mountain regions, B. Am. Meteorol. Soc., 89, 1477–1486, 2008.

Wulfmeyer, V., Behrendt, A., Kottmeier, Ch., Corsmeier, U., Barthlott, C., Craig, G. C., Hagen, M., Althausen, D., Aoshima, F., Arpagaus, M., Bauer, H.-S., Bennett, L., Blyth, A., Brandau, C., Champollion, C., Crewell, S., Dick, G., Di Girolamo, P., Dorninger, M., Dufournet, Y., Eigenmann, R., Engelmann, R., Flamant, C., Foken, T., Gorgas, T., Grzeschik, M., Handwerker, J., Hauck, C., Höller, H., Junkermann, W., Kalthoff, N., Kiemle, C., Klink, S., König, M., Krauss, L., Long, C. N., Madonna, F., Mobbs, S., Neininger, B., Pal, S., Peters, G., Pigeon, G., Richard, E., Rotach, M. W., Russchenberg, H., Schwitalla, T., Smith, V., Steinacker, R., Trentmann, J., Turner, D. D., van Baelen, J., Vogt, S., Volkert, H., Weckwerth, T., Wernli, H., Wieser, A., and Wirth, M.: The Convective and Orographically-induced Precipitation Study (COPS): the scientific strategy, the field phase, and research highlights, Q. J. Roy. Meteorol. Soc., 137, 3–30, doi:10.1002/qj.752, 2011.

Wulfmeyer, V., Branch, O., Warrach-Sagi, K., Bauer, H.-S., Schwitalla, T., and Becker, K.: The impact of plantations on weather and climate in coastal desert regions, J. Appl. Meteorol. Clim., in review, 2013.

HESSD
10, 13897–13953, 2013

Table 1. Measured quantities from Desert, Jatropha and Jojoba cases, sensor type and estimated measurement errors.

Quantity	Sensor	Estimated error
2 m air temperature (T2)	Vaisala HMP155A	@ 20 °C ±(0.055 + 0.0057 × *T*) °C
2 m relative humidity (RH)	Vaisala HMP155A	@ −20 °C +40 °C ±(1.0 + 0.008× reading) % RH
Short and long wave radiation (SW/LW)	Hukseflux NR01	±10 % for 12 h totals
6 m wind speed and direction (U and Udir)	Gill 2-D Windsonic	U ±2 % Udir 2–3°
Barometric surface pressure (BP)	Vaisala CS106	±0.6 hPa @ 0 °C to +40 °C
Soil temperatures at 5 and 25 cm (ST5 and ST25)	CS 108 Thermopile	±0.3 °C @ −3 °C to 90 °C
Soil heat flux (*G*, two plates per station)	Hukseflux HFP01	within −15 % to +5 % for 12 h totals

HESSD
10, 13897–13953, 2013

Table 2. Physics schemes used for the study within the WRF atmospheric model.

Physics	Scheme	References
Boundary layer	YSU (Yonsei University)	Hong et al. (2006)
Surface layer	MM5 Monin–Obhukov	Paulson (1970), Dyer and Hicks (1970), Webb (1970), Beljaars (1995)
Microphysics	Morrison 2-moment	Morrison and Gettelman (2008)
Shortwave radiation	RRTMG	–
Longwave radiation	RRTMG	Mlawer et al. (1997)

HESSD
10, 13897–13953, 2013

Table 3. Modifications to model vegetation parameters, based on literature, sensitivity tests and local data.

Modifications	Default Value	Prescribed Value	Source
Roughness – Z_0 (m)	0.5 m	0.3 m	Literature, canopy height
Albedo	0.12	0.12	Observations
Veg. Fraction – σ_f (%)	95 %	70 %	Local knowledge
Min. Stom. Resistance – $R_{C\,min}$ ($s\,m^{-1}$)	120	250	7th International Conference on Jojoba

HESSD
10, 13897–13953, 2013

Table 4. Modifications to model soil parameters, based on literature and local soil data.

Modifications	Default Value	Prescribed Value	Source
Soil type	Clay Loam	Sandy Loam	Local soil survey
Sat Hyd. Cond K_s ($m\,s^{-1}$)	2.45×10^{-6}	5.23×10^{-6}	Local soil survey
Porosity ($m^3\,m^{-3}$)	0.43	0.38	Local soil survey
Field Capacity ($m^3\,m^{-3}$)	0.4	0.31	Local soil survey

HESSD
10, 13897–13953, 2013

Table 5. Mean diurnal summer evaporation over Jojoba plantation based on calculations from Penman R_a/R_s and Penman 56 FAO. The values highlighted in bold are the daily ET_C or crop and canopy fraction adjusted estimates. As mean summer diurnal values were used to calculate ET the monthly figures shown are the same. In reality there may be a little variability over the summer with changing temperatures and so on.

Jojoba	Variable	Mean summer value ($mm\,d^{-1}$)
Penman R_a/R_s	ET for 100 % Canopy	6.51
	ET_c for 70 % Canopy	**4.56**
Penman 56 FAO	ET_0	8.83
	ET_c ($K_c \cdot \sigma_f$)	**4.33**

HESSD
10, 13897–13953, 2013

Table B1. Measurements of the stomatal resistances of Jojoba using different methods, at different times of day; and under varying moisture and salinity conditions. Taken from the Seventh International Conference on Jojoba and Its Uses: Proceedings (1988). See the text for individual references.

Method	Conditions	Stomatal resistance ($s\,m^{-1}$)
Heavy water scintillation	Well watered, low salt	333.3
Diffusive resistance	Well watered, low salt	625
Diffusive resistance	Well watered, high salt	1666
Diffusion porometer	Well watered, Jan	250
Diffusion porometer	Well watered, Jun	312.5
Continuous flow	Well watered, 7.00 a.m.	250
Continuous flow	Well watered, 11 a.m.	500
Unknown	Well watered, median	312

HESSD
10, 13897–13953, 2013

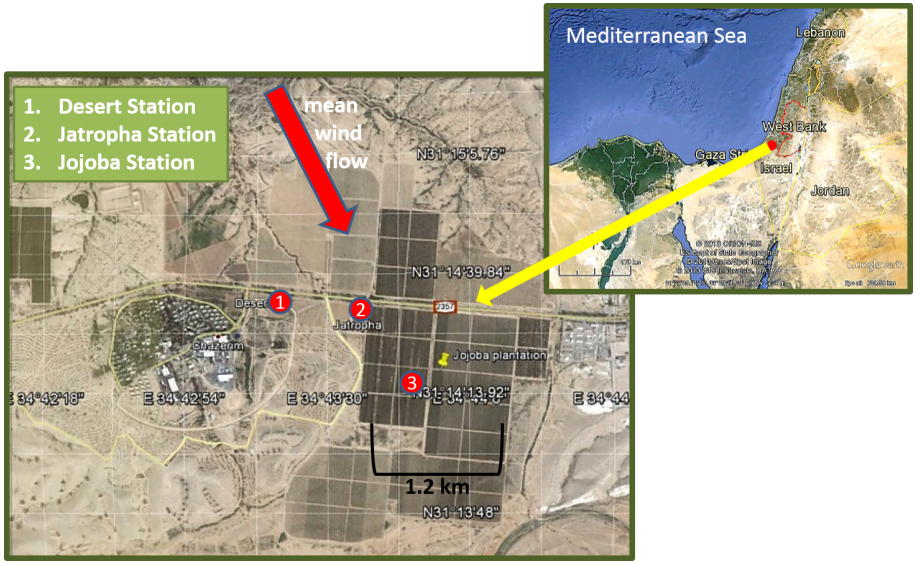

Fig. 1. The region of interest over Israel at the eastern edge of the Mediterranean Sea (inset) and the location of the 3 meteorological stations at Kibbutz Hatzerim in the centre of Israel, 40 km from the coast (the regional location is indicated by in the inset box). The location of the stations: Desert (1), Jatropha (2) and Jojoba (3) are marked on the left hand image. Mean wind flow is marked with an arrow.

HESSD
10, 13897–13953, 2013

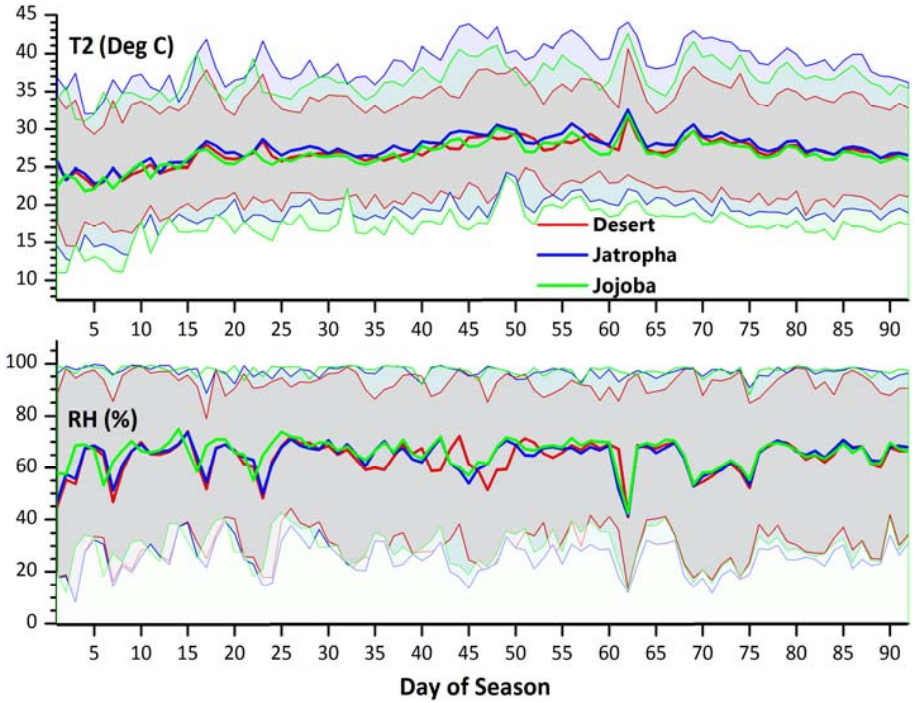

Fig. 2. Observed daily mean, maxima and minima of 2 m air temperatures and relative humidities for the Desert, Jatropha and Jojoba stations – summer 2012 (JJA). Measurements were taken 2 m over the desert surface and over the canopies. The thicker curves at the center of the shaded areas are the daily mean values. The thin lines bounding the shaded areas are daily maxima and minima.

HESSD
10, 13897–13953, 2013

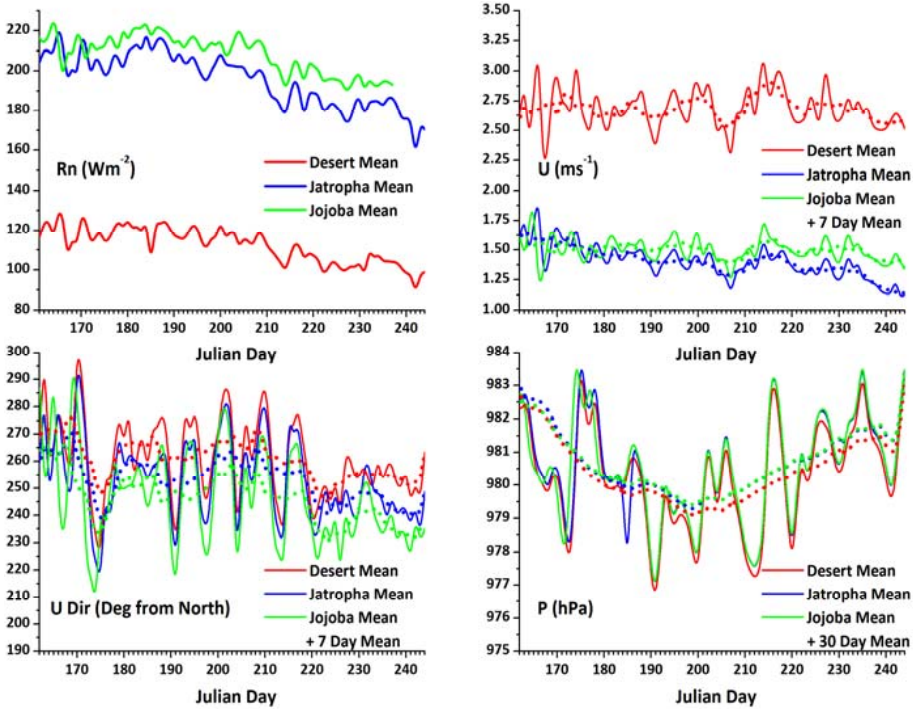

Fig. 3. Observed daily 24 h mean values of R_n, U, P, U and U direction. 7 or 30 day means are plotted as dotted lines for U, U Dir and P based on peak analysis to highlight differences between the stations and the evolution of the summer climate (2012 – JJA). Due to poor quality flags some Jojoba R_n data was rejected for the last 8 days of the season.

HESSD
10, 13897–13953, 2013

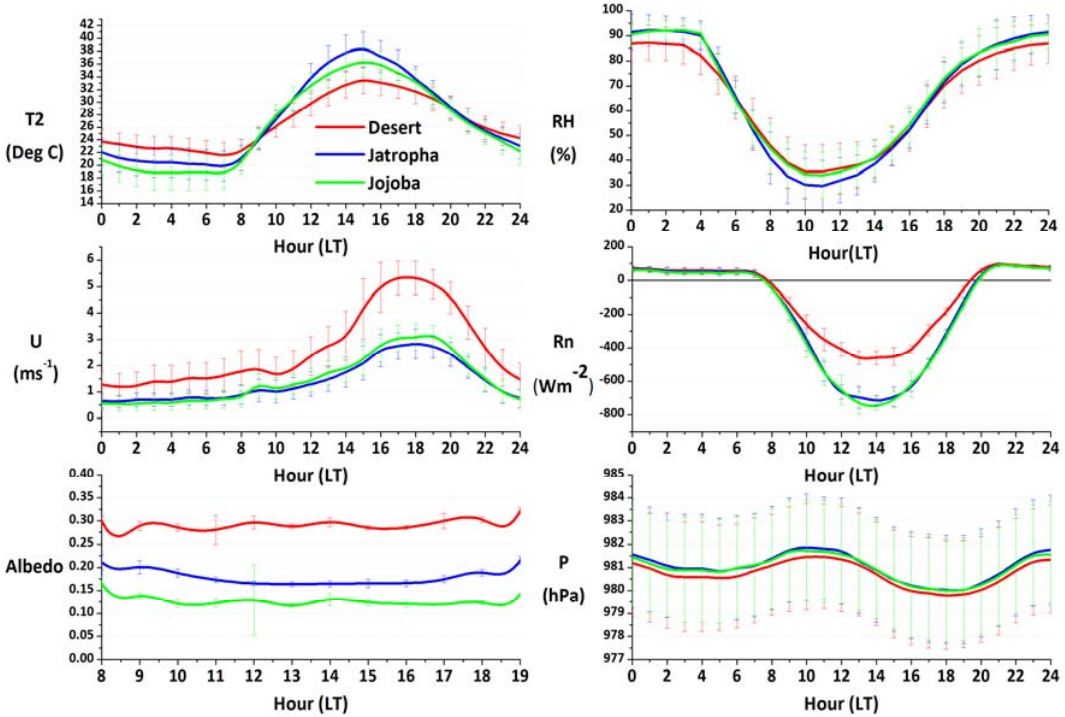

Fig. 4. Observed mean diurnal cycle of T2, RH, U (6 m), R_n, Albedo and P – 2012 (JJA). The error bars represent temporal standard deviation.

HESSD
10, 13897–13953, 2013

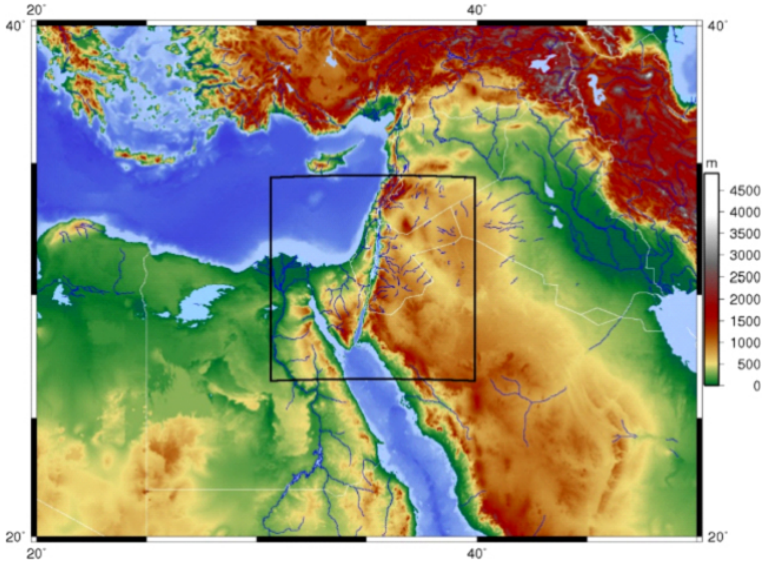

Fig. 5. Topographic map of the region of interest, at the eastern end of the Mediterranean. The model domain (approx. 888 km × 888 km) is marked in the centre with a black line. Care was taken to include synoptic features such as the NNE sea airflow into Israel, and also to avoid strong features at the boundaries, such as orography.

HESSD
10, 13897–13953, 2013

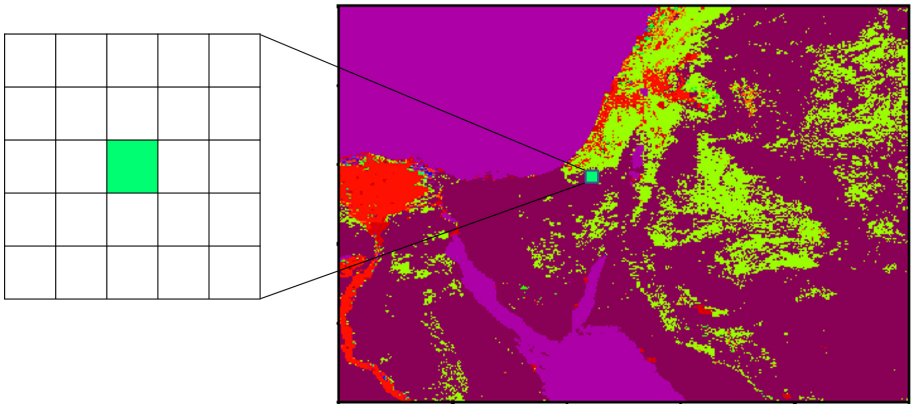

Fig. 6. Setup of the analysis of WRF output data. The image on the right is of the 20 category 30 arc second MODIS land use dataset, a static dataset for model initialisation (all 25 cells are classed as Desert/scrub in the MODIS data). A 25 cell grid box (left panel) was used, over which all variables values were averaged spatially, prior to the calculation of temporal statistics. Cell *X*, marked in bright green corresponds to the location of the three surface stations. The 25 cell box (10 km × 10 km) was also used as a template for the simulated plantation.

HESSD
10, 13897–13953, 2013

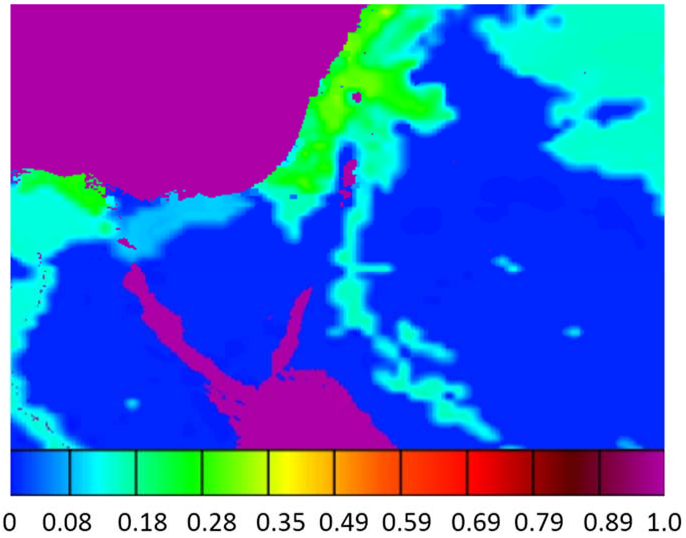

Fig. 7. ECMWF soil moisture initialisation data for the second soil layer in NOAH (10–40 cm). The re-initialisation of the soil moisture within the plantation can be seen on the image just to the left of centre where there is a small blue patch which is much drier than the surroundings.

HESSD
10, 13897–13953, 2013

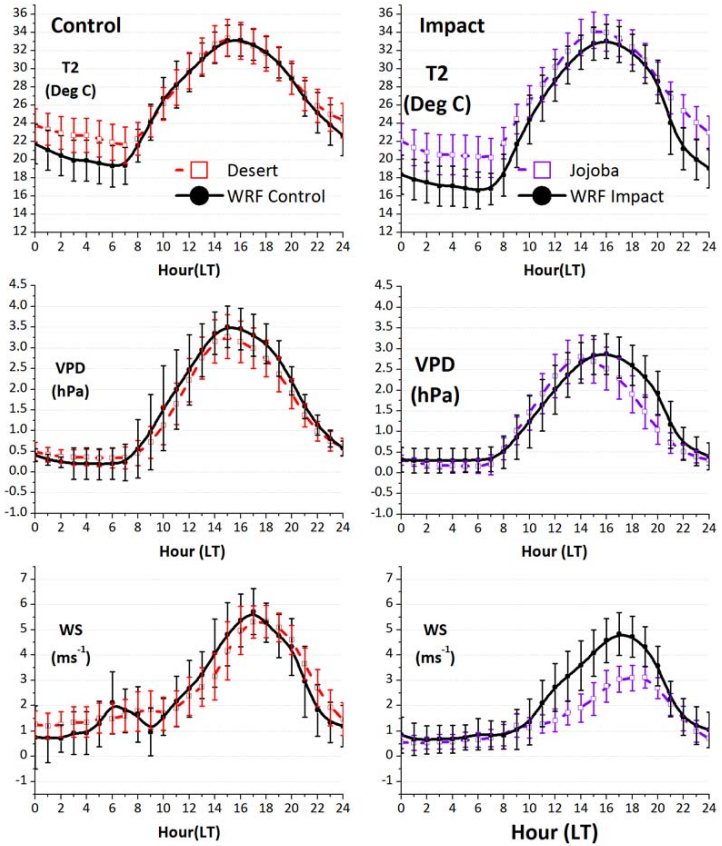

Fig. 8. Validation of WRF Control and Impact with observations for mean summer diurnal cycles of 2 m temperature (T2), 2 m vapour pressure deficit (VPD), wind speeds (U). Left hand panels show Control and the right panels, Impact. WRF variables were averaged over a 25 grid cell box centred at the geographical coordinates of the Desert, Jatropha and Jojoba sites. Note: the model wind speeds are at 10 m height, whilst the observations are measured at 6 m.

HESSD
10, 13897–13953, 2013

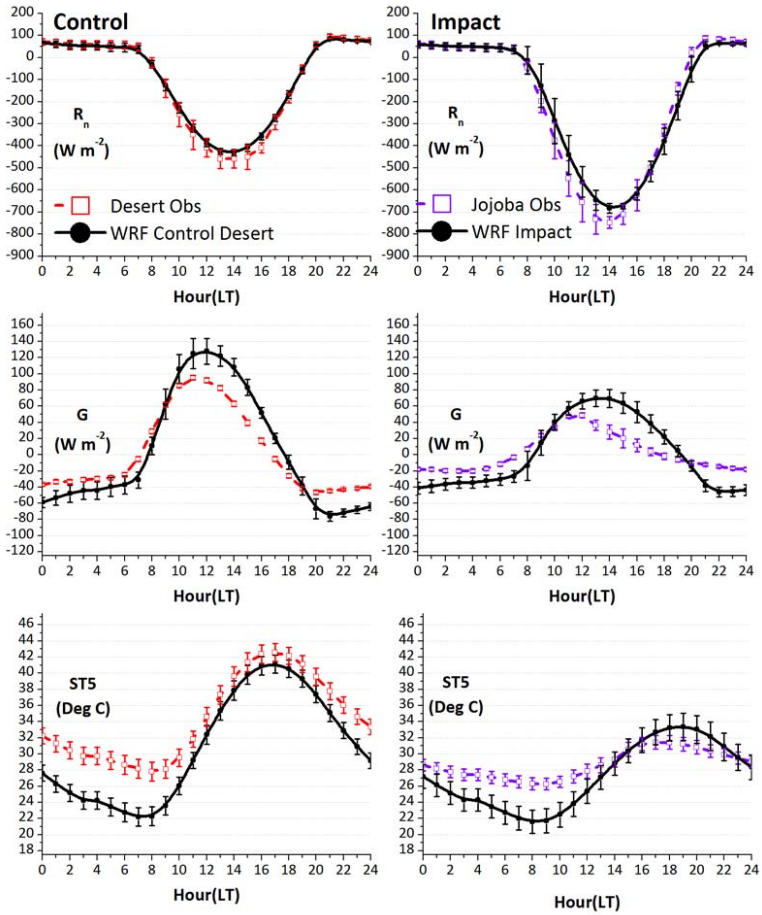

Fig. 9. Validation of WRF Control and Impact with observations for mean summer diurnal cycles of net surface radiation (R_n), ground flux (G) and 5 cm soil temperatures (ST5).

HESSD
10, 13897–13953, 2013

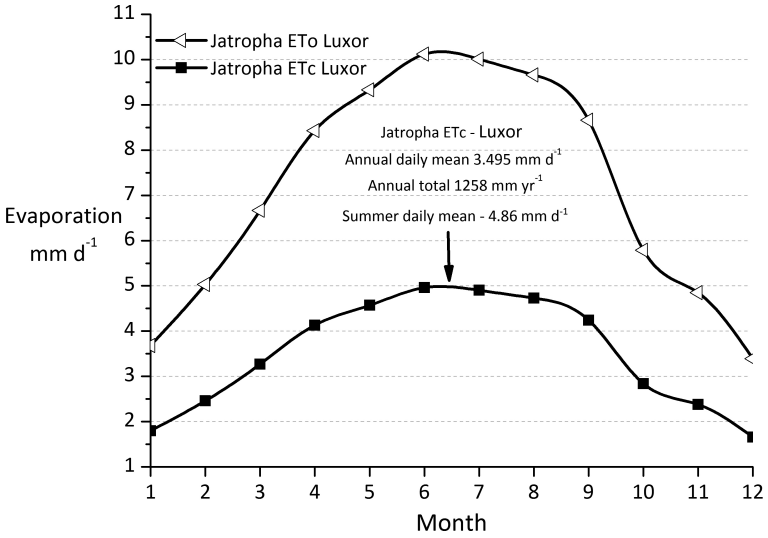

Fig. 10. ET_0 and ET_C values obtained for a Jatropha plantation in Luxor as reported in a US-AID report *Irrigation and Crop Management Plan*. The ET_C is calculated using the Penman–Monteith FAO 56 method and a crop coefficient K_C of 0.7 for Jatropha. The annual total is calculated as 1258.61 mm yr^{-1}

HESSD
10, 13897–13953, 2013

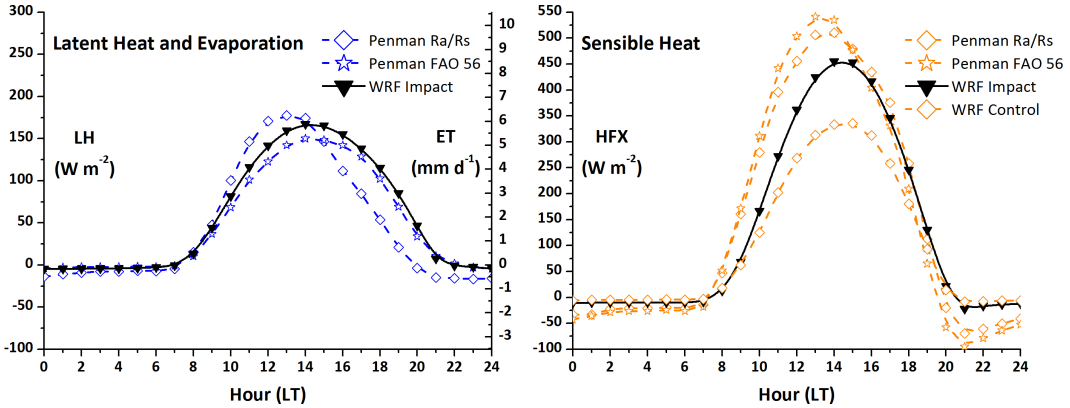

Fig. 11. Mean summer diurnal cycles of LH and HFX from WRF Impact (solid lines). Also indicated are the estimates from Penman–Monteith with R_a/R_s and Penman–Monteith FAO 56 (dashed lines). The left hand plot shows ET expressed in $\mathrm{W\,m^{-2}}$ (left y axis) and $\mathrm{mm\,d^{-1}}$ (right axis). Mean daytime values for $\mathrm{ET_C}$ are $3.66\,\mathrm{mm\,d^{-1}}$ (Penman Ra/Rs) and $3.58\,\mathrm{mm\,d^{-1}}$ (Penman 56 FAO). The right hand plot shows the HFX fluxes from WRF Impact and also the implied HFX based on the Penman estimates [calculated as the residual of the energy balance $R_n(\mathrm{Obs}) - G(\mathrm{Obs}) - \mathrm{LH(Estimation)}$]. HFX from WRF Control is also plotted to assess the diurnal differences between HFX from desert and from irrigated plantations.

HESSD
10, 13897–13953, 2013